2015

Characterization, fabrication, and analysis of soft dielectric elastomer actuators capable of complex 3D deformation

William Lai
Iowa State University

Characterization, fabrication, and analysis of soft dielectric elastomer actuators capable of complex 3D deformation

by

William Lai

A dissertation submitted to the graduate faculty

in partial fulfillment of the requirements for the degree of

DOCTOR OF PHILOSOPHY

Major: Engineering Mechanics

Program of Study Committee:

Ashraf F. Bastawros, co-Major Professor

Wei Hong, co-Major Professor

Thomas J. Rudolphi

Ran Dai

Pranav Shrotriya

Iowa State University

Ames, Iowa

2015

TABLE OF CONTENTS

ACKNOWLEDGMENTS

I would like to thank my committee members, Dr. Ashraf F Bastawros, Dr. Wei Hong, Dr. Thomas J Rudolphi, Dr. Ran Dai, and Dr. Pranav Shrotriya for their guidance and support throughout the course of this research. I would especially like to thank Dr. Wei Hong for his advises in programming and finite element analysis and Dr. Ashraf Bastawros for his full support and trust in my countless peculiar ideas and always patiently guiding me to practice my ideas in real experiments.

In addition, I would also like to thank my colleagues, the department faculty and staff for making my time at Iowa State University a wonderful experience.

Finally, I would also like to thank my friends and family for listening to my ups and downs on a daily basis. It has been a fun, fruitful, and memorable journey.

ABSTRACT

Inspired by nature, the development of soft actuators has drawn large attention to provide higher flexibility and allow adaptation to more complex environment. This thesis is focused on utilizing electroactive polymers as active materials to develop soft planar dielectric elastomer actuators capable of complex 3D deformation. The potential applications of such soft actuators are in flexible robotic arms and grippers, morphing structures and flapping wings for micro aerial vehicles.

The embraces design for a freestanding actuator utilizes the constrained deformation imposed by surface stiffeners on an electroactive membrane to avert the requirement of membrane pre-stretch and the supporting frames. The proposed design increases the overall actuator flexibility and degrees-of-freedom. Actuator design, fabrication, and performance are presented for different arrangement of stiffeners. Digital images correlation technique were utilized to evaluate the in-plane finite strain components, in order to elucidate the role of the stiffeners in controlling the three dimensional deformation. It was found that a key controlling factor was the localized deformation near the stiffeners, while the rest of the membrane would follow through.

A detailed finite element modeling framework was developed with a user-material subroutine, built into the ABAQUS commercial finite element package. An

experimentally calibrated Neo-Hookean based material model that coupled the applied electrical field to the actuator mechanical deformation was employed. The numerical model was used to optimize different geometrical features, electrode layup and stacking sequence of actuators. It was found that by splitting the stiffeners into finer segments, the force-stroke characteristics of actuator were able to be adjusted with stiffener configuration, while keeping the overall bending stiffness. The efficacy of actuators could also be greatly improved by increasing the stiffener periodicity. The developed framework would aid in designing and optimizing the dielectric elastomer actuator configurations for 3D prescribed deformation configuration.

Finally, inspired by the membrane textures of bat wings, a study of utilizing fiber reinforcement on dielectric elastomer actuators were conducted for the mechanical and the coupled electromechanical characteristics. Woven fibers were employed on the surface of actuator membrane with different pre-deformed configurations. Experimentally, actuator stiffness changes were measured for up to four orders of magnitude. The orientation of embedded fibers controlled the level and the triggered phase of stiffness changes. A trade-off between the actuator stiffness and stroke could be controlled during the fabrication stage by the fiber orientation and the prestretch level of the base elastomer membrane. A simplified model using small-strain composite laminate theory was developed and accurately predicted the composite actuator stiffness.

Additionally, compliant edge stiffeners were found had to present a marked overall effect on actuator electromechanical response.

The developed simplified analytical solutions using Timoshenko-bimaterial laminate solution and composite laminate theory, as well as the developed finite element framework can be utilized in addressing more complex 3D deformation patterns and their electromechanical response.

CHAPTER 1. INTRODUCTION

This thesis is focused on the study of flexible robotic systems utilizing soft electroactive polymers (EAPs). Dielectric elastomer is the primary EAP material employed in this study and served as the actuator backbone. Research starts with study of historical actuator designs and material characterization, followed by purposing new actuator design that answers noted device setbacks in literatures. The detail of actuator fabrication procedures as well as actuation performance evaluations are provided in Chapter 3. The study of actuation mechanism and design optimization from both macro- and micro-scale aspects are discussed in Chapter 4. Besides, the investigation of mechanical and electromechanical effect of surface reinforcements on soft actuators are included in Chapter 5. This thesis not only contributes to device design but also accomplishes thorough experimental and numerical study of dielectric elastomer actuators that may apply to aero and biomimic robotic devices.

In this chapter, the background of soft biomimic actuator development is briefly reviewed. Also, the current actuator challenges as well as the motivation of our work are discussed.

1.1 Background of Soft Actuator Development

Since the industrial revolution in the 18th century, every day, scientists and engineers are working on new devices to solve a current real-life problem and improve productivity in the industry. Historic human-made robotic systems were mainly manufactured to be utilized in assembly lines and mostly designed to be stiff and strong so that they can perform fast and precise tasks [1, 2]. Thus, the majority of actuators in such systems are built with rigid components (such as steel and aluminum alloys) and structures (such as truss backbones) to achieve the demands.

By contrast, our Mother Nature is built with all sorts of soft matters and flexible structures. In fact, the majority of animals and plants are soft-bodied [3], and even creatures with stiff exoskeletons like insects or woody plants like trees and shrubs have joints and internal tissues that are mainly composed of soft matters and liquids [2]. Besides, living things are born to perform highly complex locomotion with their flexible and deformable body structures to adapt complicated and unpredictable environments [2, 4].

These unique features have drew large interests of scientists to learn from nature that may provide invaluable insights for next generation robotic applications. Researchers are anticipating to develop next generation robots that can handle complex interactions in unstructured environments and unexpected situations [1, 5]. Soft robotics are aimed to bring up high flexibility and high degree-of-freedom motion by utilizing

structural morphology and soft material properties. There are the two major research aspects of this growing area of study: stricture and material.

From the structure aspect, actuator developments surround the idea of morphing geometry that incorporate soft materials shell [4]. Instead of building machines using hard materials truss, compliant materials are utilized to mimic motions from animals, such as elephant trunks [6], octopus arms [7-9], or caterpillars [10, 11]. These animals present almost infinite degree-of-freedom rotations with their joint-less body structures that are very different from traditional jointed rigid robots. They are generally in tube shape and able to provide either curling or squirming for gripping or locomotion [3, 5, 10-14]. One of the successful actuation approaches is employing air pressure to control the deformation [2]. Air pressure is compressed into compliant pneumatically tubes with pneu-net (PN) architecture [13, 15] to achieve tentacle bending and crawling (Figure 1a). The other approach is combining active materials, such as shape memory alloys with soft robotic bodies. Active materials can be embedded in the core of hollow elastomer shells [16, 17] or covering the cylinder shape actuators in mesh form [16, 18, 19] to control the actuator motions (Figure 1b and c).

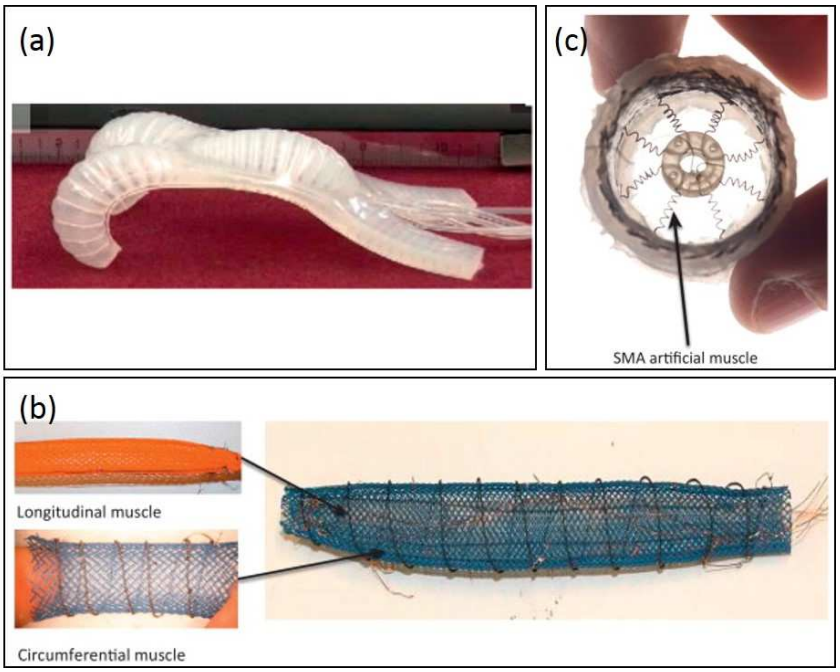

Figure 1. Soft actuators utilizing flexible structure approaches. (a) Air pressure stimulated compliant pneumatically tubes with pneu-net (PN) architecture [13, 15]. (b) Cylinder shape actuators in mesh form [16, 18, 19] to control the actuator motions. (c) Embedded active materials in the core of cylinder actuators [16, 17].

From the material aspect, scientists are focusing on functional materials, or so called smart materials, that are capable of deforming though variety of stimulations. Historically, stiff functional materials like shape memory alloys of piezoelectric ceramics have been utilized in many robotic applications [16, 19-21]. However, because of their stiff mechanical characteristic, we need to modify the structure (such as into coil or mesh form [16-19]) in order to apply to soft robotic system development. On the other hand, a group of soft active polymers can be stimulated through the inputs of electric field [22, 23], magnetic field [24], pH [25-27] or temperature [28], or even light [29, 30]. They are mostly soft and light-weight and very suitable to imitate the activities of animal muscles by themselves or being embedded smart flexible structures discussed above.

1.2 Motivation

We are interested in developing soft actuators for biomimic robotic applications. One of our main motivations is to contribute to the research of micro aerial vehicles (MAVs). In nature, bats and small birds, such as swallows, are our role models for designing tailless MAVs [31] wherein the aforementioned attributes can be engineered. They are lack of vertical tails; however, they utilize the wing dihedral and twist effectively for flying control. The dihedral (up-and-down flapping) angles of both wings can be varied symmetrically to control the flight speed of gliding or perching flight

independently of the angle of attack and fight path angle, while an asymmetric dihedral setting can be used to control yaw in the absence of a vertical stabilizer to enable agile maneuvers. Equipped with flexible wings, birds are capable of agile flight in constrained and unpredictable environments. From the engineering point of view, aerial vehicle structured with tailless body and flexible wings are usually lighter than geometrically similar rigid wings. Also, they tend to be more flexible in flying to adapt constrained environments.

To contribute to soft flexible actuator development, utilizing active polymers is a practical approach. Among which, electroactive polymers (EAPs) have been proved to be very suitable material candidates that featuring compliancy and large deformability [23, 32]. In this study, we choose dielectric elastomers, a type of EAPs, to develop soft polymer based actuators due to the advanced properties they provide. The development allows us to move toward building micro aerial vehicles with the flexible wing architecture that with benefit of lighter weight, higher energy-to-mass ratio, and greater adaptability as advanced future micro aerial vehicles.

1.3 Current Challenges

Working toward the goal of fabricating planar soft actuators capable of complex morphing ability for MAV application, it requires thorough studies from fundamental

material characterization and structures analysis to system performance evaluation. In current dielectric elastomer based actuators development, there are several challenges found in literatures. One of the problems occurred to be the additional equipment which are used to support prestretches of elastomers. Prestretch has been proved to improve actuation of dielectric elastomer actuators [33, 34]. However, the total actuation strain is limited to the extent of the prestretch; otherwise the actuator membrane would wrinkle. Besides, the supporting skeletal frames are much heavier and occupied much larger space than active polymers, thereby, reducing the actuator stroke-to-weight ratio as well as enlarging unwanted device size [35, 36]. The rigidity frames also lower the flexibility of soft polymers which contradicts the purpose of employing compliant active materials at the first place. As a result, it is a challenge to develop a freestanding actuator that eliminates the requirement of prestretch but remains great deformability and actuator performance at the same time.

Another topic being studied in this thesis is surface reinforcements applied to the soft actuators. Surface reinforcements can be served as deformation guidance to the actuators that leads the device actuation as well as property modifiers that adjust mechanical and electromechanical characteristics. In the following chapters, an actuator design with actuation mechanism that involves surface reinforcements is purposed, fabricated, and analyzed. First, we employ surface patterned stiffeners as the main driving architecture to achieve a freestanding planar actuator that remains yielding large

rotation motion without the requirement of prestetch. The observed stiffener-membrane interaction are evaluated and analyzed and could be used for designing actuators with controllable characteristics. Second, inspired by bat wings which featuring their thin and highly deformable structure that benefits the most from aerodynamics [37-41]. We apply meshing fibers on dielectric elastomer actuators similar to anatomic observation of bat wings. We are interested in learning the mechanical and electromechanical characteristics changes that influenced by such unique surface reinforcements. This could be utilized for understanding the effect of surface mechanical treatment and adjusting actuators for specific operating environments.

1.4 Thesis Outline

The ultimate goal of developing soft actuators is having efficient output force and not sacrificing great flexibility. The core value of this thesis will be working toward this direction and collaborating these two important characteristics.

In chapter 2, a literature review will be given to introduce overview of current soft actuator designs followed by materials review and selection. A variety of approaches of developing soft actuators in literatures are introduced, including both structure aspect and material aspect. Next, different electroactive polymer materials are induced and summarized, including working mechanism and their pros and cons. Among which,

dielectric elastomers are our primary of active polymers choice in this thesis. The review of dielectric elastomer actuators will be emphasized and further explored in the latter sections of this chapter. Starting with material characteristics, electromechanical properties and material nonlinearity of dielectric elastomers will be addressed. Different actuator designs as well as the related scientific issues and challenges will be reviewed including prestretch, failure mode, and numerical models. In chapter 3, a design of a planar dielectric elastomer actuator capable of complex out-of-plan deformation with no requirement of prestretch is presented. The design of geometrically confining reinforcement and the fabrication procedure will be addressed. The resulting structures enable complex 3-dimentional motions without the requirement of the prestretch and the additional supporting equipment comes along. An in-situ imaging system was used to capture the 3D deformation pattern to evaluate the actuation. The deformation mode was analyzed analytically using the bi-laminate theory to develop a closed form representation amenable for control strategies. Surface displacement analysis was performed by employing digital image correlation technic to determine actuator deformation both locally and globally. Also, a finite element material model was developed to couple the applied electric field to the resulting deformation. The model is capable of being utilized for advance complex deformation pattern analysis and for further overall device performance assessments. The proposed confining reinforcement strips mechanism would enable the development of flexible continuous robotics, utilizing

combination of the proposed deformation mechanisms to provide controllable many degrees of freedom.

Chapter 4 is devoted to the detail discussion of the confining reinforcement strips employed in our actuator design. The local effect upon surface reinforcement and elastomer interface is addressed to further study the interaction between stiffeners and active membranes. The observations are utilized to improve the developed analytical model and the understanding of the role of confining strips is employed to adjust force-stroke characteristics of actuators. The results provide the actuator with higher efficacy, better performance, and more flexible characteristics adjustment of the planar dielectric elastomer actuators and may achieve more practical applications in soft flexible wings robotic systems.

Chapter 5 is focusing on surface reinforcement applications inspired by bat wings which featuring their highly deformable structure. Meshed woven fibers are applied on dielectric elastomer actuators similar to fibrous structures on bat wings. Mechanical and electromechanical properties are examined to characterized actuators under mechanical surface modification. The understanding of surface fiber effect are used to adjust specific characteristics from electromechanically coupling representation. Laminate theory was used to predict the terminal effective modulus of fiber-elastomer composites. Different fiber patterns as well as different reinforcement materials were employed to complete thorough analysis.

CHAPTER 2. LITERATURE REVIEW

This chapter will begin with a brief introduction of electrode active polymers (EAPs) followed by an overview of some of the most commonly seen EAP materials. The general performance, advantages, limitations, and area of applications of these materials are introduced. The second part on this chapter is devoted to a review of different actuator designs purposed in literatures based on utilizing dielectric elastomers, the major interest EAP materials in this thesis. The design review includes system actuation mechanisms as well as introduction to prestretch, which is a procedure that commonly utilized for the purpose of increasing actuator performance. The pros and cons of prestretch are discussed at the end of the section. The third part of this chapter is focusing on the review of actuation failure. Failure modes and the studies of wrinkling, which is a phenomenon that strongly linked to actuator failure are addressed. Finally, three major hyperelastic material models wildly used in literatures are introduced. The governing equations as well as the applications and limitations of each of the models are illustrated.

2.1 Electroactive Polymers

Electroactive polymers are polymers that demonstrate deforming ability when employed to electric-field stimulation. They have drawn great interests for applications to artificial muscles and biomimic robotic systems [23, 42]. Compare to the majority of active materials utilized for actuator developments in the history, such as shape-memory alloy (SMA) [16, 19, 43] and piezoelectric materials [44, 45], typical electroactive polymers exhibit larger shape change during activation. Besides, the compliancy of soft polymers is able to provide great flexibility for constructing actuators with higher degree-of-freedom [23].

Many different types of electroactive polymers were purposed in the literatures. These polymers can be classified into two major categories based the activation mechanism: ionic EAPs and electronic EAPs [46]. Brief overview of the most common types of EAPs in these two categories is given in the following sections.

2.1.1 Ionic EAPs

The actuation of ionic EAPs relies on the activities of ions in polymers during activation. The ionic activities can be referred to ion exchange that occurs in chemical reactions or ion migration that driven by external applied charges. The ionic migrations typically require comparably small driving force; therefore, the operating voltage level of ionic EAPs is usually low (under 10 volts [46-48]). However, because of the high

dependency of ion diffusion, ionic EAPs generally have much slower response time than other types of EAPs [47, 49-51].

2.1.1.1 Conductive Polymers

Conductive polymers (CPs) are conducting organic materials that allow ion's (usually positive charges) migration inside materials. They were first introduced by Baughman et al. [51] and became active material candidate for actuator development. The actuation of conductive polymer based actuators is found on electrochemical reaction that different ionic activities will be introduced under oxidation and reduction. A typical actuation structure includes two conductive polymer layers and an electrolyte layer in between. Conductive polymer layers are connected to positive and negative electric potential individually that will correspondingly urge oxidation or reduction. To balance the charges, flux of ions will move in and out of the conductive polymer backbones and cause volume changes resulting in deformation. The anode layer will swell and the cathode layer will shrink due to the ionic migration and the stacking laminates will bend toward the cathode side as a result. Although actuation voltages of conductive polymer are low (1-2 volts [12, 51]) and may introduce strain from 2% to up to 20% [51], this type of EAP is suffering from low operating efficiency (~1% [12]). In addition, since the actuation is highly depended on ion diffusion between polymer chains, the response time is strongly related to polymer network orientation [46, 51] as well as mobile ion density [46] and, as a result, the deformation rate is usually comparably slow (12%/s) [12]. Most

of the application of conductive polymers are in the field of biosensors where they are considered as a suitable material for enzymes to enhance speed and sensibility [52].

2.1.1.2 Ionic polymer-metal composites (IPMCs)

Ionic polymer-metal composites (IPMCs) were initially proposed by Oguro et al. [53] and soon followed by ongoing extensive studies. Typically, IMPCs are constructed with an ion-exchange polymer membrane sandwiched by two thin flexible metal (typically platinum or gold) electrode layers with thickness around 3-10 nm [47]. The particular ion-exchange polymer, 3M Nafion® 117 from DuPont for example, only allows the migration of cations. Therefore, while applying voltage (normally lower than 10 volts), mobile ions in the polymer membrane will flow toward anode of the IPMCs [47] and cause non-symmetric volume distribution. As a result, bending (with strain around 3% [47]) can be observed as shown in Figure 3.

IPMCs work very well in air as well as in a liquid environment due to the hydrophobic feature of the polymer backbones [46]. They are able to generate a tip force of almost 40 times their own weight in a cantilever mode. Similar to other ionic EAPs, IPMCs have had been suffering from slow response time as well as deformation rate due to the ionic-diffusion related deformation mechanism. However, R. Montazami et al. [54] purposed an idea of applying three layered structure, (two porous composite electrode layers conductor network composites, CNC) and significantly improved actuator performance with an actuation response time around 0.2 seconds. The major applications

of IPMCs are in flapping or swimming robotic motion in air and hydraulic environments [12].

2.1.2 Electronic EAPs

The actuation of electronic EAPs relies on electric field that directly empowers polymer shape changes. Typically, the changes may be coming from the inner transformation to the polymer microstructures related to chain orientations or outer transformation to the polymer blocks related to physical compression caused by electromechanical coupling effect that physically compresses a piece of polymer sample. Since the deformations of electronic EAPs are directly introduced by electrostatic forces (such as Maxwell stress [55]), their response time is comparably fast but usually required much higher operating voltage [12, 46].

2.1.2.1 Ferroelectric Polymers

Ferroelectric polymers are considered as analogous to ferromagnets, where the application of an electric field aligns polarized domains in the materials [12]. Since the permanent polarization exists even after the field is removed, the deformation of ferroelectric polymers is able to remain without continuous electro field applied. Ferroelectric EAPs can be operated in air, a vacuum, or water in a wide range of temperatures typically between 20 and 80 °C [12]. Poly (vinylidene fluoride-trifluoroethylene) (P(VDF-TrFE)) is a commonly used ferroelectric polymer which has a

strain observation up to 7% and an elastic energy density above 1 MJ/m3 under an electric field of 150MV/m and a strain as high as 2% under a low applied field about 13 MV [42].

2.1.2.2 Dielectric Elastomers

Dielectric elastomers are soft polymers with comparably high dielectric constant for suitable electromechanical coupling effects. They can be utilized to build dielectric elastomers actuators (DEAs) and applications to actuators and sensors have drawn great interests since R. Pelrine et al. firstly presented their study [33]. A dielectric elastomer actuator is typically made of an incompressible soft dielectric elastomer membrane sandwiched by compliant electrodes. When an electric field is applied across the plates, the laminate works as a dynamic capacitor, and the stress generated from columbic force (so called Maxwell stress [55]) attracts both electrode layers together. Electrodes squeeze the sandwiched incompressible elastomer membrane and result in structural planar expansion due to Poisson's effect (see Figure 4). The electric field induced Maxwell stress can be described as, $\sigma_{Maxwell} = \varepsilon\Phi^2$, where ε is the material permittivity (material dielectric constant multiples the vacuum permittivity) and Φ is the applied electric field.

Typically, silicone or acrylics are utilized as the dielectric elastomer materials and conductive particle solutions, such as carbon grease or metal partial paints are utilized as the electrode materials. Although the operating voltage of DEAs is high (~1-10 kV), the current range is less than several milliamps that leads to very small amount of working power. The actuation strain is considerably high that over 100% of deformation can be

achieved [12, 56-58]. One of the other benefits of dielectric elastomers is the material availability. Several inexpensive commercialized products, such as Dow Corning HS3 silicone, NuSil CF19-218 silicone, BJB Enterprice TC-5005 A/B-C silicone, and 3M VHB 4910 acrylic tapes [12] have shown successful results in literatures. Noted that the performance of dielectric elastomer actuators can be effectively improved by applying "prestretch" on the elastomer membrane [33, 34]. Detail of the study of prestretch will be addressed in the following sections.

Dielectric elastomers are very suitable for actuators with light weight, high flexibility, and reasonable response time. Therefore, we choose dielectric elastomers as the primary EAP materials for prototyping actuators in the field of MAV application study.

2.2 Dielectric Elastomer Actuator Designs

Many different soft actuator design based on dielectric elastomers w purposed in literatures. There are two major categories of design that were presented in the past: (a) actuators with hard frame for supporting prestretch, and (b) using prestretch as stored energy for the recovering of bi-stable structures. This section will start with introducing prestretch followed by an overview of different dielectric elastomer actuator design in the literatures.

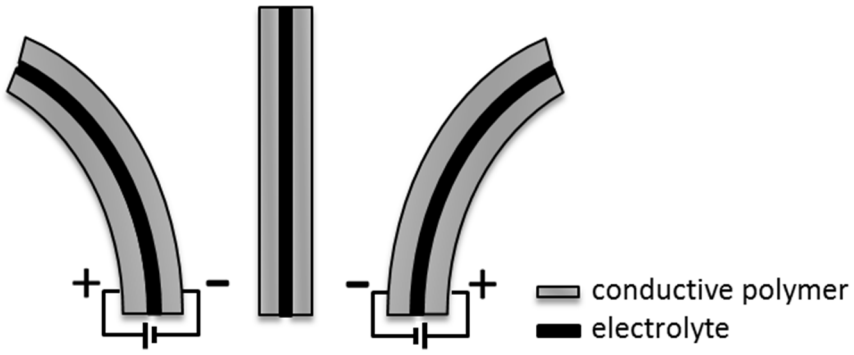

Figure 2. Sketch of actuator based on conductive polymer sandwich structure showing bending mechanism founded on oxidation and reduction of polymers.

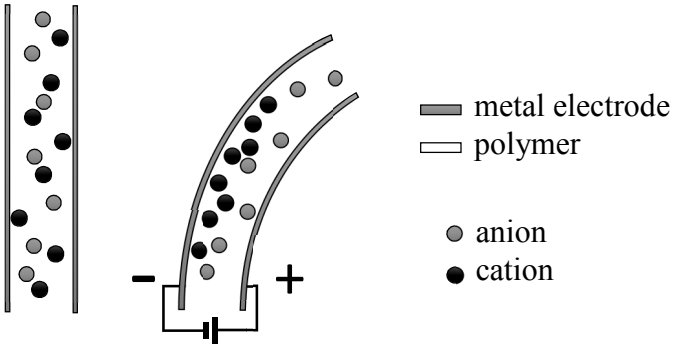

Figure 3. Sketch of IPMC mechanism. When applying voltage, mobile ions, cations, in the polymer membrane will flow toward anode of the IPMC.

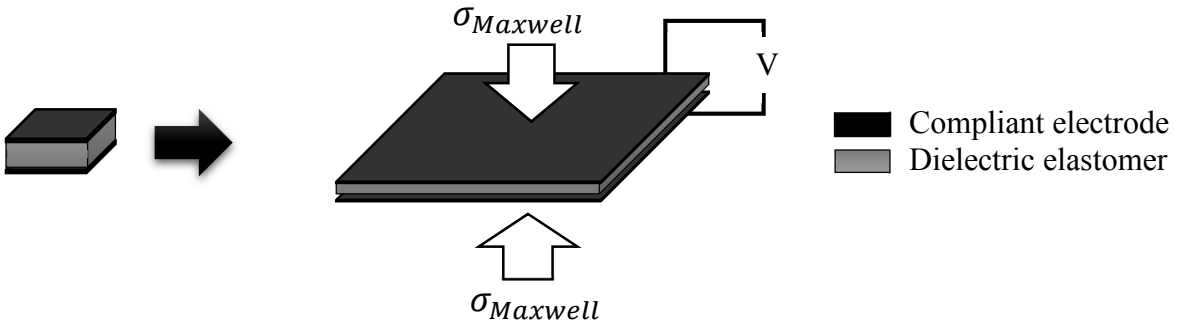

Figure 4. Sketch of dielectric elastomer actuator (DEA). Sandwich structure of 2 compliant electrode layers and a dielectric elastomer membrane. When an electric field is applied, Maxwell stress will induce in-plane expansion due to incompressibility of the elastomer membrane.

2.2.1 Prestretch

Prestretch has been shown to successfully improve the in-plane actuation of dielectric elastomer actuators [33, 34] that an actuator made of elastomer membranes with prestretch can achieve more than 300% of strain. Prestretch is a procedure that apply residual tension on the elastomer membrane. The pre-deforming process is thinning down the membrane so that the operation voltage level can be decrease to fulfill the required electric field. Also, when the actuator is activated, the elastomer membrane is under compression on the thickness direction due to Maxwell stress. If the membrane is fitted on an outer frame, it will as well undergo compression on the in-plane direction due to Poisson's effect. This may cause instability to the actuator and induce actuator failure which can be prevented by the tension applied on the membrane through prestretch. Finally, prestretch changes the stretch-voltage characteristics of a dielectric elastomer actuator [46, 59]. It lowers the barrier of instability and induce a smoother phase transition that does not involve a jump-through deformation, or so called pull-in failure [60], that exceeds theoretical breakdown electric field. More detail of voltage-stretch characteristics is discussed in section 2.4 where numerical models are introduced.

However, prestretch requires additional structure for holding the tension on membranes and the additional supporting frames tend to cause operational setbacks. For example, weight and space that the support structures occupied are much more than dielectric elastomer itself [36, 57]. In addition, non-uniform prestretch and stress

relaxation may affect subsequent actuation [61] and cause local strain division that influenced by non-uniform prestretch and the biaxial prestretch ratio. Besides, the usage of rigid frames contradicts the gold of developing soft actuators with high flexibility. These setbacks limit the application of dielectric elastomer actuators. In the following sections, actuator designs in the literatures that adapt prestretch with different methods are discussed.

2.2.2 In-plane Actuators

Because of the natural actuation mechanism, dielectric elastomer actuators are able to directly introduce in-plane expansion on a membrane. For a prestretched dielectric elastomer membrane that is fixed on a rigid outer frame with electrodes deposited partially on the surface, regional expansions can be seen on the area with electrodes ion the surface during activation. One of the major actuator designs based on the in-plane expansion is a rotation device serve as a generator. This design is called a dielectric elastomer generators (DEG) which was first purposed by the team from University of Auckland [62-64]. The working mechanism behind the design is utilizing regional expansion on the membrane to further induce position displacement on the surrounding area. That is to say, when a small region on a dielectric elastomer actuator is activated, the activate area will expand and the surrounding area will move outwards along the normal strain direction. With series of sub block around a target spot deposited with electrodes discontinuously (see Figure 5), the position of target spot can be controlled as

a sequel by activating the surrounding block one-by-one. The motion of this center spot is outled by an extended bar so that a rotation generator is able to be applied.

The other design found on in-plane expansion of dielectric membrane is a stiffness-control system [65] allowing a 7 to 10 times change in stiffness that can be applied to a passive spring and a stiff motor in applications such as landing gears of airplanes [66]. As the purposed device structure shown in Figure 6, passive compliance adjustment is able to be achieved through controlling membrane tension. As mentioned in the prestretch section, activate a stretched dielectric elastomer actuator, the compression caused by Maxwell stress will reduce the residual tension on the membrane due to prestretch. Applying different level of voltage leads to different level of membrane tension and, as a result, changes the system stiffness response as shown in see Figure 6c.

The last design application is a tensile force transmission device by utilizing out-of-plane compression that occurs with in-plane expansion [67]. Different from the applications mentioned above, this design employs out-of-plane shrinking of the membrane that accompanies with expansion. Normally the thickness shrinkage is too small to be neglect as the thickness of the membrane is too small. However, by stacking layers of actuators into a long pillar, a maximum of 30% of non-loaded contraction can be achieved and a 10% of contraction with lifting 1 kg of mass can also be observed at activation. The manufacturing process of stacking DEAs are further studied in literatures where utilizing folding method is shown to be an easy approach of fabrication [67, 68].

This system design can be used in mimicking muscle contraction as backbones of tentacle actuators.

2.2.3 Actuator with Flexible Joints

With prestretch applied on elastomer membrane, supporting frames are required to withstand the tension. A way to build flexible actuator with the rigid frames is to instructing flexible joints. The flexible joints can be several movable junctions within a frame or hinges in between series of actuators. A robotic-arm design that S. Dubowsky et al. purposed [69] showed a configuration of adding deformable corners on the prestretch-supporting frame of a planar actuator. This allows a frame-included linear deformation during actuation instead of an in-frame-only movement. By combining multiple units of actuator on different orientations, higher degree of freedom motion can be achieved on a platform that is constructed on these actuator legs.

The other approach was presented by Lochmatter et al. [70] for a shell bending actuator. The actuator structure is fundamentally constructed with a pair of parallel segments. The actuation of two planar actuators are controlled separately that by activating one of the paired actuator, an asymmetrical bending motion can be achieved. The larger scale of shell-like structure includes hinges in between planar actuators so that multiple actuators are connected together on each side. By controlling each of the actuators individually, a possible multiple degree of bending and swinging of the shell is provided.

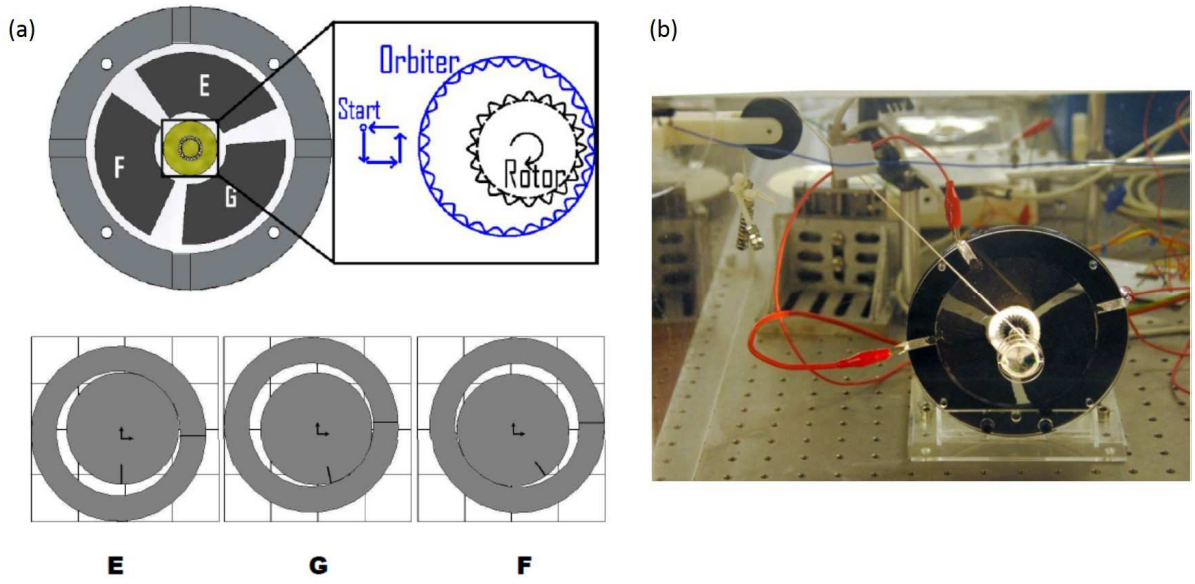

Figure 5. (a) Sketch of a dielectric elastomer actuator based soft rotary motor showing that the rotation motion can be introduced by sequentially activating different region of the area (region E, G, F). (b) A real setup of a soft rotary motor. [64]

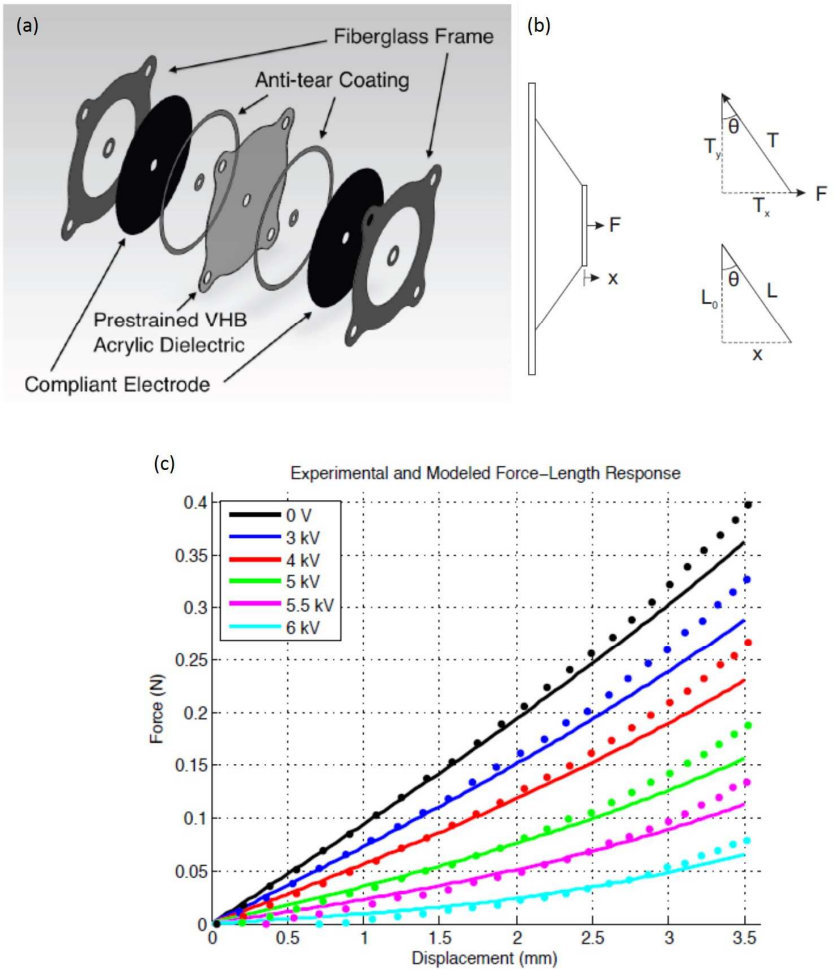

Figure 6. (a) Exploded view of device assembly. (b) Side view of the device under normal stress applied on elastomer membrane with membrane tension breakdown. (c) Variable stiffness response through applying different voltage. [65]

2.2.4 Dielectric Elastomer Minimum Energy System

Another design to perform out-of-plane deformation from a prestretched dielectric elastomer actuator is named dielectric elastomer minimum energy system (DEMES) which first purposed by G Kofod et al. [71]. The design demonstrated a strategy to repeatedly utilize prestretch as a stored energy with its bendable frame that used to support prestretch. This structure has bi-stable configurations that occur before and during actuation. First, elastomer membrane is prestretched and fixed on a hollow frame made of thin paper of plastic sheet. When releasing the system to freestanding, the membrane will crumble to compensate the stored energy from prestretch. With prestretched elastomers attached on deformable frames, actuators may stay in relaxation phase where elastomers are crumbled under no electric field applied. And when the actuators are activated, they may deform into the other stable phase where the energy from applied electric field overcomes the stored energy provided by prestretch and makes elastomer flat. Later, Petralia and Wood further presented their work of a curving chain actuator by combining several paper-frame-based DEMES cells. This design is highly dependent to the geometry transformation and has shown applications in bender of gripper by employing different frame design.

2.3 Actuator Failure Modes

This section is focusing on different causes of actuator failure as well as visual phenomenon accompany with it. The actuator failure may be due to mechanical limitation, electrical limitation, or the combination of two that occurs under a snap-through transformation from material stability [60]. The mechanism of each failure mode is discussed as following.

2.3.1 Mechanical failure

Mechanical failure is related to the limitation of martial strength. During activation, if the expansion excesses the larger stretch that a material can tolerate, it is obvious that the membrane will break and the actuator will fail. In experiments, this type of failure is not commonly seen, since most of the elastomer membrane employed in dielectric elastomer actuator are highly stretchable. Actuators tend to fall into other categories of failure before they reach the maximum extensibility of materials.

2.3.2 Electrical breakdown

The breakdown electric field of a dielectric material is a material constant and the breakdown voltage limit can generally be obtained experimentally. When the applied electric field is too high, it empowered the dielectric material to become conductive. The excessed electric filed may be caused by the applied voltage becomes too high or the thickness of elastomer membrane becomes too thin. Once the elastomer membrane

becomes conductive, the positive and negative electrodes on both surface are connected. This will short and burn the membrane and result in actuator failure.

2.3.3 Instability

Another name for instability failure is called pull-in [60]. It appears when the equilibrium condition of electric field and Maxwell stress cannot be reached. Maxwell stress is proportional to electric field square by definition, and it is also the driving force of compression that induce the in-plane expansion of elastomer membrane as well as the thickness shrinkage. On the other hand, electric field is proportional to the applied voltage and the membrane thickness. That is to say, when applying a voltage to the actuator system, the real electric field will fall into an increasing loop that caused by the shrinkage of membrane thickness from actuation and may end up with electrical breakdown. Prestretch plays an important role here to improve actuator performance as it can adjust the voltage-stretch characteristics.

2.4 Numerical models

Several numerical models have been purposed in literatures to describe the hyperelastic material behavior. In addition to linear Hook's law that may be applied to materials under very small deformation, three of the most common nonlinear models used for dielectric elastomers are Ogden model, Neo-Hookean model, and Gent's model.

They are employed case by case according to different actuation situations and operation stretch ranges of actuators. An overview of these three nonlinear model is discussed as following.

2.4.1 Ogden model

Ogden model was developed by Dr. Ray W. Ogden in 1972 [72] for complex non-linear stress-strain behavior of materials such as rubbers and polymers which are generally considered as incompressible. The model includes 1 or higher order terms of material constant that can accurately describe rubber-like materials but fitting material parameters. The elastic energy in Ogden model can be written as $W = \sum_{p=1}^{N} \frac{\mu_p}{\alpha_p}\left(\lambda_1^{\alpha_p} + \lambda_2^{\alpha_p} + \lambda_3^{\alpha_p} - 3\right)$, where N, μ_p, α_p are material constants. For particular values of material constants, the high order of Ogden model will reduce to either the Neo-Hookean or other solid material models. Despite the accuracy, Ogden is very complicated for time-efficient numerical simulation. It is a perfect model to represent dielectric elastomer mechanical behavior observed in experiments within all the stretch range [56, 57, 73], but not the first model choice to apply in numerical analysis.

2.4.2 Neo-Hookean model

Neo-Hookean is a material model with linear stress-strain relation based on Hook's law and geometric nonlinearity for materials under large deformations [74]. Neo-Hookean model utilizes stretch instead of strain to describe material mechanical

properties. The elastic energy in Neo-Hookean model can be written as $W = \frac{\mu}{2}\left(\lambda_1^2 + \lambda_2^2 + \lambda_3^2 - 3\right)$, where μ is the shear modulus of the material and λ_i is the stretch on each axis. In terms of principal stretches, stresses for an incompressible material like dielectric elastomer can be describe using principal stress differences as following.

$$\sigma_{11} - \sigma_{33} = \lambda_1 \frac{\partial W}{\partial \lambda_1} - \lambda_3 \frac{\partial W}{\partial \lambda_3};\ \ \sigma_{22} - \sigma_{33} = \lambda_2 \frac{\partial W}{\partial \lambda_2} - \lambda_3 \frac{\partial W}{\partial \lambda_3}$$

Therefore, by applying the elastic energy into the equations,

$$\sigma_{11} - \sigma_{33} = \mu\left(\lambda_1^2 - \lambda_3^2\right);\ \ \sigma_{22} - \sigma_{33} = \mu\left(\lambda_2^2 - \lambda_3^2\right)$$

As shown, the only required material variable to describe a dielectric elastomer is the shear modulus, which is able to ease the computational work significantly. Neo-Hookean model works perfectly under lower range of stretch and is also suitable to apply in smaller stretch range by fitting the shear modulus. It can, however, only describe the initial compliancy of rubber and polymer chain behavior. More complicated inter-polymer-chain behavior is not able to be represented via this model. Nevertheless, the simplicity is very suitable to employ in finite element analysis for fast numerical simulation, especially for our actuator design which only involves comparably small initial stretches.

2.4.3 Gent model

Gent model [75] can be considered as an advanced Neo-Hookean model that also utilizing material shear modulus to represent the stress-strain relationship of the material. In addition, an additional term, $J_{\lim}$, is introduced to describe the concept of limiting polymer chain extension. $J_{\lim}$ is a material constant related to the material extensibility that caused by straighten polymer chains [75, 76]. The elastic free energy in Gent model can be written as $W = \frac{-\mu J_{\lim}}{2} \ln\left[1 - \frac{\lambda_1^2 + \lambda_2^2 + \lambda_3^2 - 3}{J_{\lim}}\right]$, where μ is the shear modulus of the material and λ_i are the stretches on given axes. When the material is under small stretches or $J_{\lim}$ is infinite large, Gent model is considered identical to Neo-Hookean model. Whereas when the material is under large deformation reaching near the limitation of polymer chain extensibility, material stress-stretch behavior will show a secondary sharp stiffening that dominated by the straighten polymer chains.

For the purpose of studying electromechanical coupling responses in a dielectric elastomer actuator, voltage-stretch curves are often employed to represent actuator behavior. According to the free-body diagram shown in Figure 7 of a dielectric elastomer actuator under applied electric field and prestretch caused by external load *P*, the equilibrium state of an active dielectric elastomer actuator can be written as the following equations coupling electromechanical responses:

$$\sigma_1 + \varepsilon\Phi^2 = \lambda_1 \frac{\partial W}{\partial \lambda_1}$$
$$\sigma_2 + \varepsilon\Phi^2 = \lambda_2 \frac{\partial W}{\partial \lambda_2}$$

Where σ_1, λ_1 and σ_2, λ_2 are the stresses and stretches on the in-plane expansion directions, σ_3, λ_3 are the stresses and stretches on thickness direction that electric field is applied through, and Φ, ε, W are applied electric field, permittivity, and elastic energy respectively. Because of the incompressibility, we know that $\lambda_1\lambda_2\lambda_3 = 1$. Therefore, the deformed thickness of the elastomer membrane during actuation is equal to $\frac{H}{\lambda_1\lambda_2}$ where H is the original thickness. By applying all the parameters, we can interpret the observed actuation behavior under applied voltage V by the following governing equations:

$$\frac{\lambda_1 P_1}{HL_2} + \varepsilon\left(\frac{\lambda_1\lambda_2 V}{H}\right)^2 = \lambda_1 \frac{\partial W}{\partial \lambda_1}$$
$$\frac{\lambda_2 P_2}{HL_1} + \varepsilon\left(\frac{\lambda_1\lambda_2 V}{H}\right)^2 = \lambda_2 \frac{\partial W}{\partial \lambda_2}$$

A voltage-stretch curve of a dielectric elastomer actuator under prestetch condition induced by load P and applied electric field introduced by voltage V can be therefore plotted.

Utilizing voltage-stretch, the experimental observation of how prestretch improve actuator performance by eliminating pull-in failure can be explained. Take an actuator under equal biaxial prestretch as an example [59], the voltage-stretch shown in Figure 8 illustrates prestretch changes electromechanical characteristics of actuators by lower the

first peak of actuation. Under no or low prestretch, when applied voltage is reaching a critical value, actuator is undergo a snap-through deformation and landed beyond the material electrical breakdown state. Therefore, no intermediate actuation stretch can be observed which leads to limited expansion and sudden failure. Using Gent model, voltage-stretch curves shrift upwards with higher material stiffness and the second stiffening kink which represents maximan polymer chain extendibility will shift toward left with higher J_{lim} that indicates smaller deformability of the system.

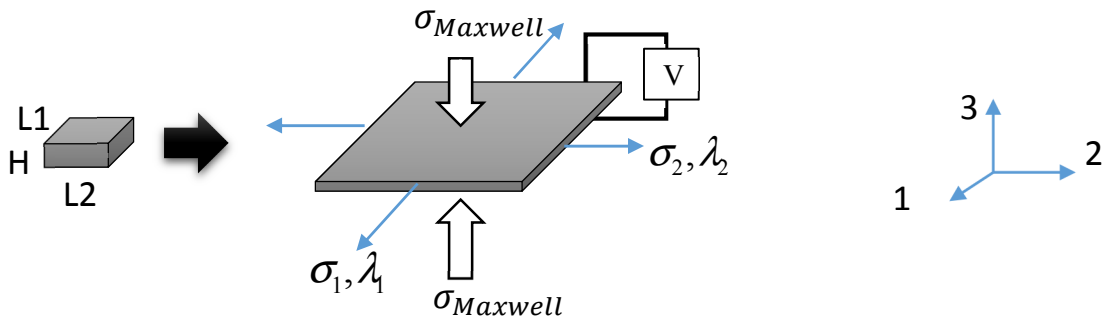

Figure 7. Free-body diagram of a dielectric elastomer actuator under applied electric field and external prestretch and stress components. Illustrating the equilibrium state of an active dielectric elastomer actuator.

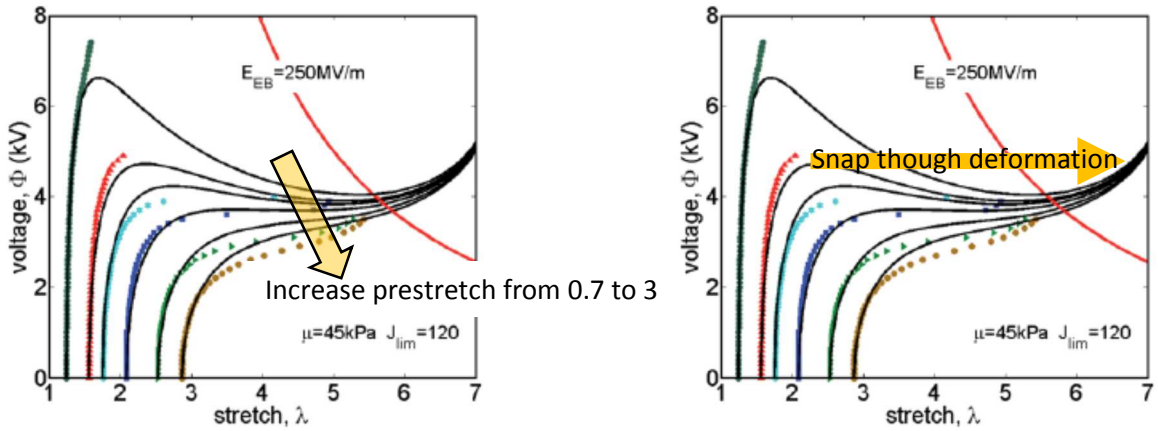

Figure 8. Voltage-stretch plots showing experimental results (dotted lines) and fitting Gent model (solid lines) and how prestretch interact with pull-in instability of dielectric elastomer actuators [59].

CHAPTER 3. PERFORMANCE OF PLANAR DIELECTRIC ELASTOMER ACTUATOR WITH STIFFENERS FOR LARGE ROTATIONAL ACTIVATION

3.1 Introduction

Electroactive polymers (EAPs) is a group of smart materials that provide considerable deformation through electric-field stimulation [22, 23, 77, 78]. Among the different classes of EAPs, dielectric elastomers exhibit high stretch-ability, comparably short response time, low cost, and high electromechanical coupling efficiency.[12, 23, 46, 79] They are often fabricated into dielectric elastomer actuators (DEAs) in the form of a sandwich structure with an incompressible soft dielectric elastomer core and compliant electrode skin, and thereby composing a dynamic capacitors structure. When electric field is applied across the electrodes, electrostatic force (so called Maxwell stress [55]) is generated, attracting both electrode layers together. The electrodes effectively squeeze the incompressible dielectric elastomer layer and result in planar expansions due to Poisson's effect.

Various designs of dielectric elastomer actuator have been purposed. The most common designs incorporate either a hard frame [46, 69, 70, 78] that allows planar actuation within the limits of the frame, or a compliant frame that can provide laarge

rotation [36, 71]. For example, Dubowsky et al. presented a robotic-arm design with rigid frames connected by deformable joints to support prestretch [69], and to allow the dielectric elastomer membrane to expand during activation. Several cells of actuators can be combined together for multi-degree-of-freedom motion. Such design represents a semi-freestanding actuator capable of device position adjustment, such as macroscopic rotation. On the other hand, compliant frames would enable transition for bi-stable actuator structures, such as dielectric elastomer minimum energy system (DEMES) [71]. By attaching a pre-stretched elastomer on a flexible planar -frame, the frame would assume a 3D shape to minimize total elastic energy of the combined membrane-frame actuator structure. When the dielectric elastomer is electrically activated, large rotational degrees of freedom would arise and recover the 3D geometry to a flat planar configuration. Such bi-stable configuration is controlled by both the stored elastic energy and the applied electrostatic energy. This concept is further utilized in a curving chain actuator [36] by combining several paper-frame-based DEMES cells.

Employing flexible or rigid frames facilitate dielectric elastomer prestretch to provide an effective method for achieving larger in-plane actuation strain of DEAs [32, 34]. However, these frames pose limitations on actuator weight, actuator size, as well as flexibility [80, 81]. As an alternative for membrane prestretch, this work presents another design of dielectric elastomer actuator with embedded soft stiffeners, instead off employing prestretch and supporting frames. In-plane surface reinforcement on a thin

planar dielectric elastomer actuator is employed to provide large out-of-plane deformation. The resulting actuator structure is a bi-material laminate, with single or multiple cells. Surface constraint will cause expansion mismatch through the thickness direction, leading to out-of-plane bending rotation and dictated by the stiffeners orientation. Details of fabrication procedures and actuator performance results for different number of cells are provided. Also, details of the localized deformation pattern around the stiffeners are analyzed by digital image correlation technique. An analytical expression for the actuator deformation is developed by coupling electromechanical effect and actuator geometry. The model accounted for the observed localizations around the stiffeners through a scaling factor. The model could be utilized to provide insights on the role of stiffeners on controlling the actuator rotation, and for further overall device performance assessments.

3.2 Fabrication Procedure

The device was designed and fabricated as a square shape sandwich laminate with the size of 25mm×25mm. Each laminate was stacked up with top and bottom layers of compliant electrode (carbon black powder, Super C65, TIMCAL Inc., USA) and two layers of elastomer (3M VHB F9460PC tapes) having 50 micrometer thick and initial elastic modulus in the order of 100kPa. A 1.5mm inactive boundary is maintained to

provide sealing and inhibit short circuit and arcing near the actuator edge. Therefore the electrically active area is about 22mm×22mm (Figure 9a). Carbon black powder was uniformly brushed over a window mask which was used to define the electrode region. Additional aluminum foils were added at the edges to form the electrodes external terminals. This sequence was repeated for stacked actuator of multiple cells. The order of positive and negative terminals was flipped for successive cells to locate all positive terminals on one side of the stacked actuate and the negative terminals on the other side. The stacked planar actuator was finished with a cover layer of the VHB tape for protection. Compliant surface stiffeners were attached on top of the cover layer. The utilized stiffeners were acrylic films (3M 810 Scotch Magic Tape) of 46μm thick and elastic modulus of about 2.4GPa. The initial stress-strain curves for both the dielectric elastomers and the polymeric stiffener are shown in Figure 10 for the range of strains relevant to the operational range of the proposed actuator. These curves were derived from tensile tests at a slow loading rate of 10 micrometer per second. The stiffeners were cut into slender 3mm wide strips (Figure 9b). The stiffener width was selected to exhibit the same order of bending stiffness compared to the dielectric elastomer layer, despite its tensile stiffness is almost an order of magnitude higher than the dielectric elastomer (e.g., Figure 10). For complex curvature, different shapes and layout of stiffeners could be utilized. The completed stacked actuator is shown in Figure 9c. Side-view illustrations of 1 (which is the minimum stack of basic DEA design), 2, and 3-cell structure are shown in Figure 11a.

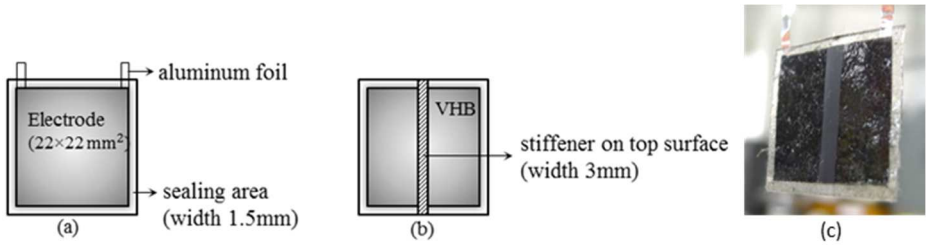

Figure 9. Illustration of the proposed stacked actuator. (a) Top view of a unit-cell actuator, showing its dimension. (b) A single strip configuration stiffener in the middle on the top surface. (c) Optical image of a freestanding actuator.

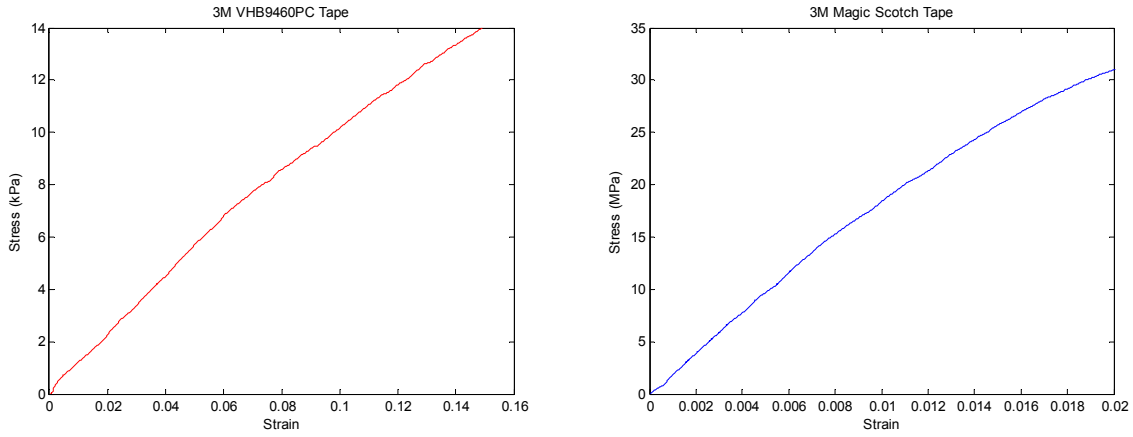

Figure 10. Stress-Strain relations for the dielectric elastomer (VHB9460 tape) and the stiffener elastomer (3M Magic Scotch tape) showing the difference in their initial elastic moduli.

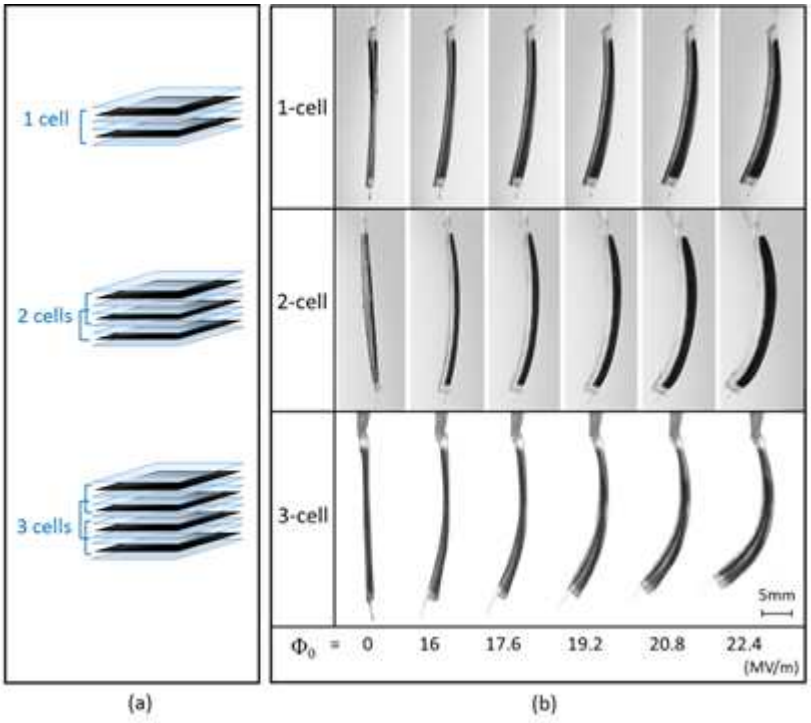

Figure 11. (a) Illustration of the stacked actuator assembly with different number of cells and with a single strip stiffener configuration. (b) Optical images of the progression of actuator curvature under different level of applied electric field; $\Phi_0 = 0 \sim 22.4\,\mathrm{MV/m}$.

3.3 Experiment

Freestanding actuators were freely supported from its electrode terminals, and connected to the high voltage driving electric circuit. The driver circuit shown in Appendix C is composed of a DC-DC voltage converter (Q-80, EMCO Inc.) with linear amplifying range of 0 to 8kV output for an input low voltage of 0 to 5V. The resistor bridge was utilized to monitor the activation voltage and the instantaneous charging current. A programmable power supply (BK Precision® 9130) is utilized to provide a controlled input voltage as a step function with different amplitude. Activation voltages in the range of 0 to 2.24kV were utilized. The actuator deformed shaped was captured by an in-situ image system having a high-resolution CCD camera (GRAS-20S4M-C, Point Grey Inc., 1624 x 1224 pixel, 14-bit gray-scale level and 30 frame/second sampling rate) and a compact imaging lens with F2. Digital images were analyzed to characterize the out-of-plane displacement of the actuator tip relative to its root, and the average overall curvature. To eliminate deformation delay caused by elastomers, images were captured 5 seconds after each voltage step where over 70% of actuation is achieved as suggested in reference [69, 82]. The experimental results of 1, 2, and 3-cell actuators with a single stiffener strip are shown in Figure 11b. The noted electric field strength is defined as the nominal electric field Φ_0 (input voltages divided by original thickness of dielectric membrane thickness for each unit cell; 0.1mm).

Figure 12 shows side view of the progression of the actuator bending deformation, for a range of electric field strength of $\Phi_0 = 0 - 2.24\,\mathrm{MV/m}$, and for actuator stacks with different number of cells. The deformed actuator curvature was assumed to be uniform and was evaluated from the cord distance between the actuator edges and the dome height at the middle of the actuator span. The measured curvature results are shown in Figure 13 for stacked actuators with different cell numbers. The effect of the number of cells can be vividly seen as increase of the overall actuator curvature for the same applied voltage. In addition, higher input electric field resulted in larger curvature bending of the actuator.

3.4 Analytical Representation of the Actuator Response

A key for prospective implementation in control strategy is to have an analytical representation of the actuator response. Here we utilized the Timoshenko's analysis of bi-material thermostats [83] under external thermal driving force. However, instead, we introducing the Maxwell stress as the external driving field to arrive at the general deformation representation under applied electric field.

When a bi-layer structure is subjected to external field (e.g. thermal or electrical), internal, self-equilibrating axial and bending stresses will be generated as shown in Figure 12. For the case of a dielectric actuator, the resulting total strain in each layer is the

summation of strains induced by the applied electric field as well as the self-equilibrating axial, and bending stresses. For the ith layer, the total strain is represented by

$$\varepsilon_{total} = \varepsilon_{electrical} + \varepsilon_{axial} + \varepsilon_{bending} = \varepsilon_{electrical}\Big|_i + \frac{1}{E_i}\frac{w_i P_i}{a_i w_i} + \frac{M_i}{E_i I_i}\frac{a_i}{2} \tag{1}$$

Here, E is the elastic modulus, a in the layer thickness and w is the layer width. We invoked here the theory of dielectric elastomer, REF-1 to arrive at the electric field induced strains. For an ideal dielectric elastomers, the active layer is assumed incompressible with Poisson's ratio, $\nu \approx 0.5$ and its permittivity $e = \varepsilon\varepsilon_o$ is a constant, independent of the deformation (ε is the dielectric constant and ε_o is the vaccum permittivity). The induced Maxwell stress due to the applied nominal electric field Φ_o is,

$$\sigma_{zz} = \varepsilon\varepsilon_o\Phi_o^2 \tag{2}$$

The resulting lateral strain within the plan of the actuator, which is $\varepsilon_{electrical}(\Phi_0)$ in Eq. (1), becomes,

$$\varepsilon_{electrical}(\Phi_0) \equiv \varepsilon_{xx} = -\nu\frac{\sigma_{zz}}{E} = \frac{\text{ö}\text{ö}_0}{2E}\Phi_0^{\,2} \tag{3}$$

Following the Timoshenko's analysis of bi-material thermostats [83], the system actuation curvature κ can be written as a function of the applied nominal electric field, the materials moduli and the laminate geometry ,

$$\kappa = \frac{\alpha \beta \frac{\dot{\alpha}_0}{2E_1} \Phi_0^{\,2}}{\frac{2}{a_1 + a_2}\left(E_1 I_1 + E_2 I_2\right)\left(\frac{1}{E_1 a_1 w_1} + \frac{1}{E_2 a_2 w_2}\right) + \frac{a_1 + a_2}{2}} . \qquad (4)$$

Here, I is the section second moment of area, and a and w are the thickness and width of each lamina. β is a geometric factor that accounts for the role of the two inactive cover layers of the actuator on the total planar expansion. Applying the strain compatibility in all layers, β was found to depend on the ratio of the active layers thickness to the total actuator thickness. For example, for the case of 1, 2, and 3-cell actuators, β is 1/2, 2/3, and 3/4 respectively. The parameter α is another geometric fitting parameter that scales the idealized analytical solution with a detailed three dimensional finite element numerical analysis. It was found that for all the applied voltage range and the different number of cells, $\alpha \approx 0.55$ would fit the prediction of the analytical expression, Eq. 4 with the entire range of the experimental results. Figure 13 summaries the experimentally measured curvature for actuator with different cell numbers with the prediction of the analytical solution, Eq. 4, under different applied electric field.

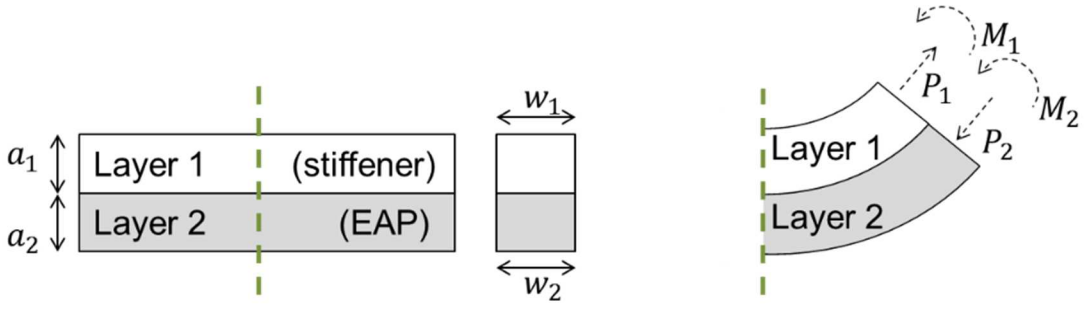

Figure 12. Free-body diagram of stiffener and EAP bi-layer structure represents planar actuator with surface reinforcement. In this figure, a is the thickness, w is the width, M is the bending moment, and P is the axial load.

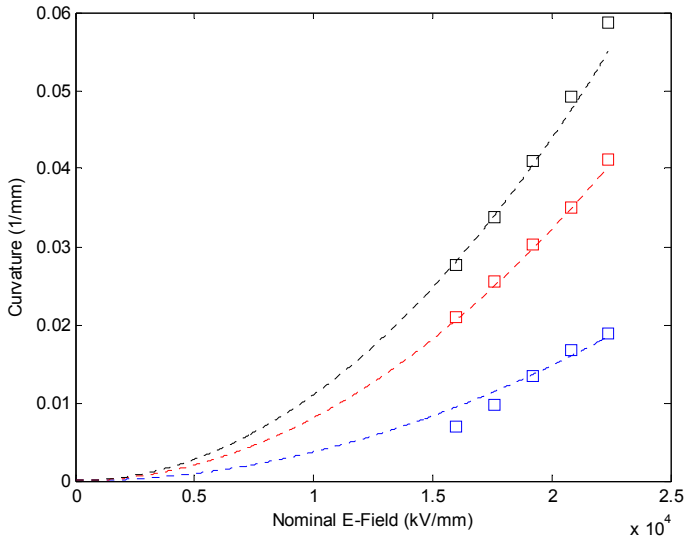

Figure 13. Comparison between the experimentally measured curvature under different level of electric field, and the derived analytical expression using Timoshenko bimaterial thermostats.

3.5 Role of stiffeners

The out of plan curvature of the actuator is primarily controlled by the embedded stiffener into the actuator. To understand the interaction between the stiffener and the actuator layer, digital image correlation (DIC) technique is employed to quantitatively analyze the deformation field. The actuator surface is decorated with white alumina powder of 1 micrometer to generate a random speckle pattern of approximately 5-10pixel per feature over the image plane (

Figure 14). Displacement field was estimated by correlating the speckle pattern in a pair of digital images before and after deformation. Commercial DIC software (Vic-2D, Correlated Solutions, Inc.) was utilized to analyze acquired imagines. A correlation window of 15pixel was utilized. The analysis grid of 7 pixel spacing was also utilized to render the two dimensional displacement vectors over the entire field of view. The desecrater displacement field over 5x5 analysis point was fitted to a third order polynomial in order to evaluate the displacement gradient and the corresponding components of the in-plan strain tensor.

Figure 14 shows the components of the in-plane finite strain distribution of a 3-cell planar actuator with single stiffener reinforcement. The strain distribution clearly shows extensive localized deformation close to the stiffener. While the strain is more uniform away from the stiffener domain. The domain of the localized deformation, which resembles a boundary layer is about 2mm or about half the stiffener's width and about

5times the actuator thickness. We speculate that boundary layer thickness is more controlled by the actuator thickness rather than the stiffener's width.

Figure 14 shows the strain distribution normal to the stiffeners. The expansion surface strain (Eyy) near the stiffeners is about three times the average level in the actuator laminate away from the stiffeners. Also, the effect of the free edge can be clearly seen. These combined effects of free edge and partial constraint condition caused by stiffeners, justify the knock-down parameter $\alpha \approx 0.55$ that was incorporated in Eq. 4 to compare the analytical solution (which assumes uniform expansion) with the experimental results.

3.6 Computational Simulation

We applied finite element method to develop a computational framework embedded in commercial finite element software ABAQUS by utilizing user material subroutine where the total free energy of dielectric elastomer actuator is defined as the summation of elastic energy and electrostatic energy. Here, incompressible Neo-Hookean material model is used to represent the elastomer behavior and the total free energy is written as a function of stretch λ and applied nominal electric field Φ_0 as equation (1)

$$W(\lambda_1, \lambda_2, \Phi_0) = \frac{1}{2}\mu\left(\lambda_1^2 + \lambda_2^2 + \lambda_1^{-2}\lambda_2^{-2} - 3\right) + \frac{1}{2}\dot{o}\dot{o}_0\Phi_0^2\left(\lambda_1^{-2}\lambda_2^{-2}\right) \quad (1)$$

The two required material properties in our framework are shear modulus and dielectric constant. The dielectric constant of VHB 9460PC tapes was defined as for 3.21 [85] and the shear modulus was found to be 0.033 MPa from performing a uniaxial tensile test. We measured the Young's modulus to be 0.1 MPa and the shear modulus was converted by applying Hooke's Law with assuming elastic deformation and incompressible material that assigned Poisson's ratio to be 0.5. We neglected thickness of electrode layers and combined all active layers into one single layer. Each separated layer was assigned with a Hybrid 20-node quadratic brick element and linked by surface-based tie constraint. 3D geometric half sample cantilever laminate was used in the model with one edge anchored and other edges left free-to-move. Two CAD models were established according to experiments where 1 and 3 segments of stiffeners were attached on the surface respectively. More CAD model detail is listed in appendix B. Curvatures were used to represent actuation motion. Curvatures were assumed as partial circles and calculated based on the in-plane and out-of-plane displacements of the central point at the end free edge. The visual deformation results of actuators with single and three stiffeners are shown in Figure 17, with respect of serial input nominal electric field up to 22.4 kV/mm. The side view of deformation sequence in simulation is shown in Figure 18. In-plane strain field of the actuation is also be obtained and shown in Figure 19.

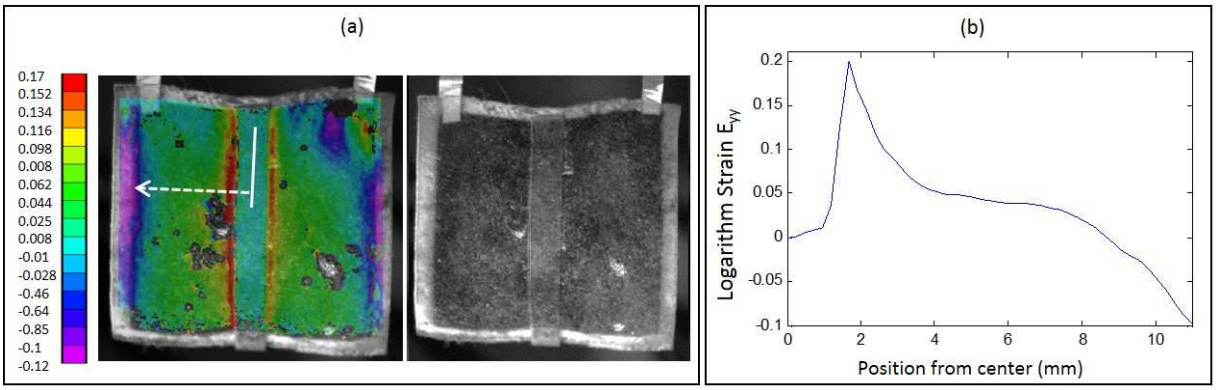

Figure 14. Experimental results on in-plane Surface Strain distribution for a 3-cell Actuator, under an applied nominal electric field of 22.4 MV/m, showing the localized inhomogeneous deformation near the stiffener. (a) Speckle enhanced surface and Eyy. Component of strain distribution along a line normal to the stiffeners. The strain near the stiffeners is about 3 times the average strain within the actuator.

3.7 Conclusion

The presented freestanding planar dielectric elastomers actuator design with embedded stiffener is capable of out-of-plane deformation. The embedded reinforcements results in complex 3D shapes without the need of supporting frames or prestretch. The strip stiffener with different stacked configuration have resulted in a scalable curvature output. A new inhomogeneous deformation mechanisms is shown with localized deformation near the stiffeners. More complex layout of the stiffeners would results in more complex 3D deformation. In-situ imaging is used to capture the electric field induced curvature. Analytical solution representing the actuator performance is developed using the Timoshenko bi-material thermostats. It is was shown that an increase of the number of active stacks in the actuator configuration would increase the driving forces that have to remain in balance with the forces generated within the stiffening layer. Digital image correlation was used to elucidate the role of the stiffeners and the details of the inhomogeneous deformation field. It was found that the strain near the stiffeners is about three times the average strain within the actuator. The developed physical understanding and analytical expression of the actuator performance could be used in future studies to modify the actuator characteristics and optimize actuator performance.

CHAPTER 4. DISTRIBUTED STIFFENERS ON PLANAR DIELECTRIC ELASTOMER ACTUATORS

4.1 Introduction

Dielectric elastomers are considered as successful material candidates for artificial muscle applications in developing soft biomimic system due to their human-muscle like features [12, 23, 50]. To apply dielectric elastomer actuators to the development of robotic systems like micro-aero vehicles, weight and energy-to-mass ratio are very important. We learn from nature that bats and small birds like barn swallows are lack of vertical tails to exchange lighter body weight. The vertical tails were usually used by flying creatures to control flying direction. Instead of holding additional tail parts, small birds and bats, however, utilize flexible wings capable of adjusting dihedral angles to guide their flying [31]. This can be a solution to provide agile flight lighter weight and adaptation in constrained environments. Dielectric elastomer actuators are very suitable for this application due to their high deformability.

In previous chapter, we have presented a promising freestanding actuator design of planar dielectric elastomer actuator (DEA) that averts the requirement of prestretch [84] and the subsequent supporting structures. Employing surface constraints on

electroactive membrane through patterned stiffeners, the proposed devices are capable of providing higher flexibility and energy-to-mass ratio. Without applying prestretch on elastomer membranes, however, potentially loses better in-plane deformation [32, 34, 73] as well as force-stroke characteristics [56, 73]. In the meantime, we observed a localized deformation occurred around the stiffener/elastomer boundary in pervious study. The majority of deformation was proceeded in this region and hypothetically dominated the overall system actuation. We assumed an effective zone is related to the localized deformation and governed by the stiffeners. The effective deformation zone may be the key for tuning actuator characteristics and improve actuator performance. Here, we purpose to maximize the effective area by changing stiffener arrangement, where a stiffener is split into several finer segments, while maintaining the device bending stiffness. Increase the periodicity of stiffeners will increase the overall effective actuation region and lead to an improved actuator performance.

This chapter will be focused on investigating the role of stiffeners. Experiments were conducted to show improved actuation by tuning the periodicity of stiffeners. Surface displacement analysis through digital image correlation technique was performed to evaluate in-plane strain component on the actuator surface. The results were used to determine the effective region and calibrate the analytical model developed in Chapter 3. A finite element framework was developed and utilized to study localized micro effects as study force-stroke characteristics of actuators with different stiffener

arrangement. The results provide an effective approach for planar dielectric elastomer actuators with better performance though tuning surface stiffener configurations.

4.2 Fabrication and Experiment

To study the role of stiffeners, we purposed to fix the system bending stiffness and vary periodicity of stiffeners. In Experiment, two cases were conducted for comparison: (a) single stiffener and (b) split stiffeners with the maintained total width. Following the detail of fabrication procedure in previous chapter, two 3-cell planar actuators that composed by stacking three unit cells were fabricated. Each unit cell includes two layers of VHB 9460PC tape (50μm thick each, 100μm thick in total) that sandwiched by compliant electrode layers where carbon black particles (Super C65, TIMCAL Inc., USA) were employed. Two additional VHB 9460PC tapes were used to cover up the stacked actuator for protection and make total thickness of 0.4mm for a 3-cell planar actuator with the thickness of electrode layers neglected (Figure 15a). One of the planar actuators was attached with one 3mm-wide stiffener (3M Magic Scotch Tapes) on the surface and the other actuator was attached with three 1mm-wide stiffeners equally separated as shown in Figure 15b and Figure 15c. Actuators were connected to the high voltage circuit with applied voltages range of 0 - 2.24kV by employing a DC-DC voltage converter (Q-80, EMCO Inc.) (Appendix C). High-resolution CCD camera (GRAS-20S4M-C, Point Grey Inc.) with 1624 x 1224 pixel, and 14-bit gray-scale level with an in-situ image system as

discussed in Chapter 3 was utilized to capture the side and front view of actuator deformations. The deformation sequence under applied nominal electric field, Φ_0 , of 0-22.4kV/mm is shown in Figure 16. Actuation curvatures were measured from the captured images assuming partial circle shapes and shown in square marks in Figure 17.

4.3 Discussion

From the experiments, we observed that the actuation curvatures are controlled by the arraignment of attached stiffeners. In the two distributed cases shown above, the total bending stiffness was controlled to be the same by maintaining the total width of stiffeners. However, the characteristics of actuators were different. With increasing the precocity of stiffeners, larger curvatures was achieved. To understand this, we went utilized finite element analysis in several aspects. First of all, if we look at the general deformation shapes shown in Figure 20, bending was not uniform. Buckling occurred between stiffeners and the end-edge of actuator. For a bending actuator, this kind of buckling is appreciated. It wastes deformation on unwanted direction (lateral direction) deformation. Increasing stiffeners is able to eliminate the unwanted deformation and keep bending more uniformly. With less waste of energy on secondary motion, larger deformation on the designed direction (axial direction of stiffeners) may be induced and results in achieving larger bending curvature.

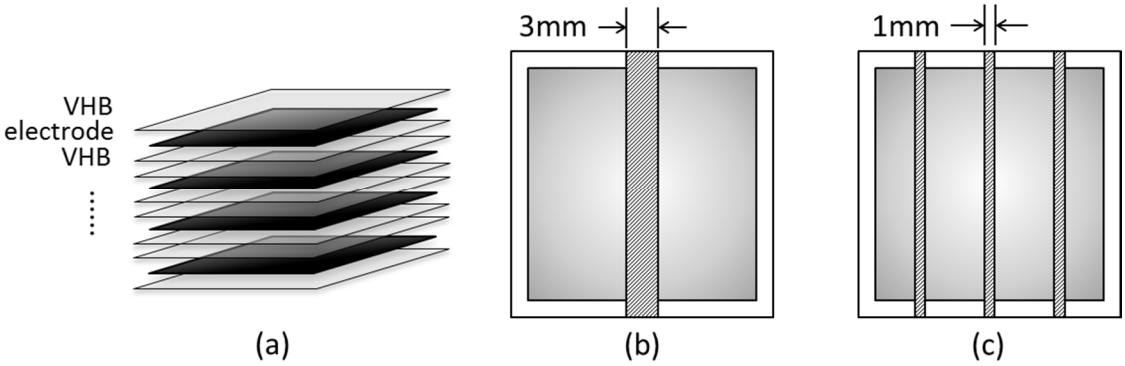

Figure 15. Schematic diagram of (a) side view of 3-cell planar actuator and two DEA samples with (b) singe stiffener and (c) triple split stiffeners attached.

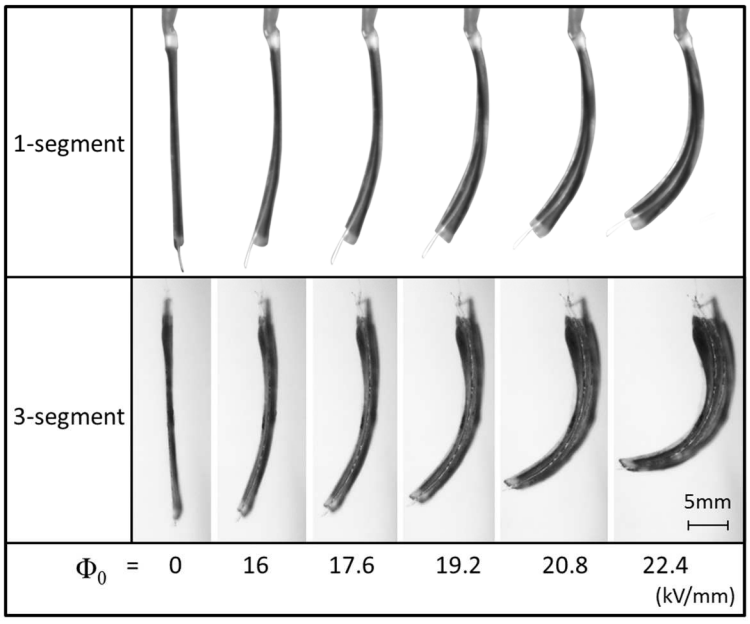

Figure 16. Experimental results of deformation sequence of 3-cell DEA with stiffener configuration of 1 and 3 segments attached under applied electric field of 0-22.4MV/m.

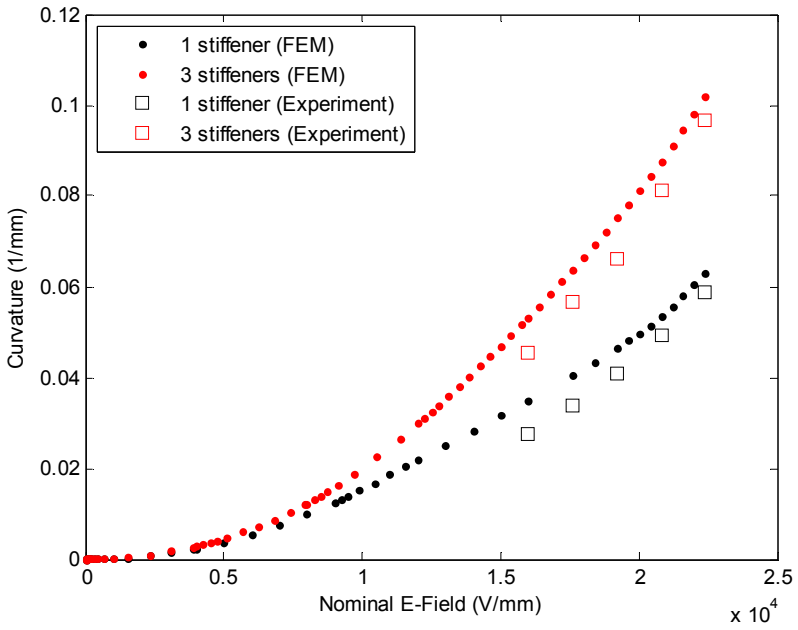

Figure 17. Actuation curvatures under applied electric field of 0-22.4kV/mm of 1 (black) and 3 (red) segments of stiffeners attached on a 3-cell DEA. Square marks and dotted lines represent results from experiments and finite element analysis respectively.

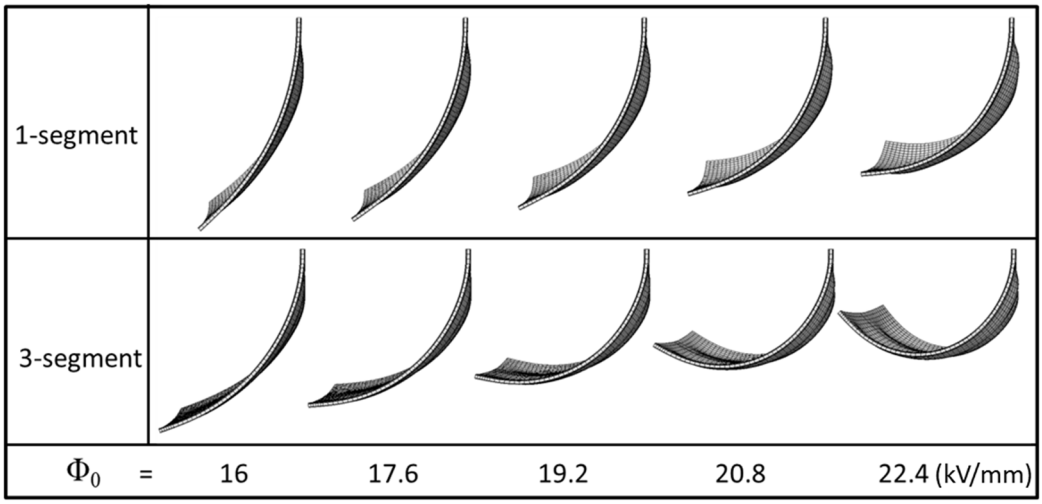

Figure 18. Deformation sequence in finite element simulation of 3-cell planar actuator with 1 and 3 segments of stiffeners under nominal electric field of 0-22.4 kV/mm.

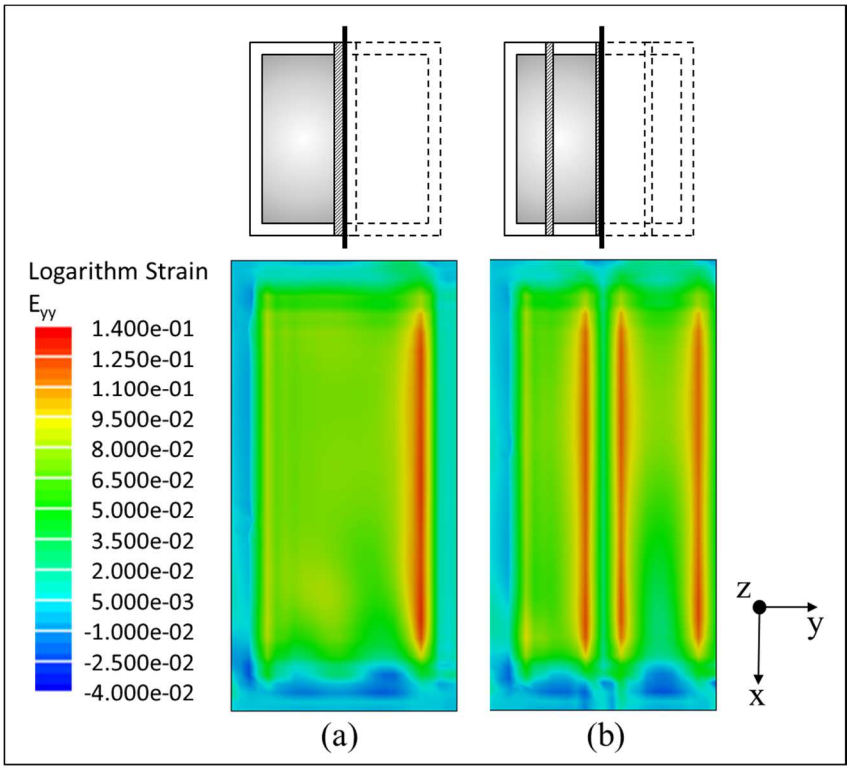

Figure 19. Strain field of 3-cell planar actuator with 1 segment (a) and 3 segments (b) of stiffener under nominal electric field of 22.4 kV/mm.

Secondly, reviewing analytical analysis in the previous chapter, we represented actuation curvatures κ as a function of input nominal electric field Φ_0 combined with actuator geometric parameters as in equation (2), where $\dot{\alpha}\dot{\alpha}_0$ is dielectric constant of the elastomer multiplies vacuum permittivity; E, I, and a are Young's modulus, moment of inertia, and the layer thickness; subscripts 1 and 2 represent layer stiffener and layer dielectric elastomer respectively. h is the total thickness and δ is a geometry factor that varies with the amount of laminated cells due to the actuator design.

$$\kappa(\Phi_0) = \frac{1}{\rho} = \frac{\beta\delta \frac{\dot{\alpha}\dot{\alpha}_0}{2E_1} \Phi_0^{\,2}}{\frac{2}{h}\left(E_1 I_1 + E_2 I_2\right)\left(\frac{1}{E_1 a_1 w_1} + \frac{1}{E_2 a_2 w_2}\right) + \frac{h}{2}} \tag{2}$$

Here, an extra fitting parameter β was required to fit the analytical model to our experimental measurements. Originally in the analytical model, we assumed uniform deformation through then entire surface. However, stiffeners in our design are not fully covering and, as a result, only affect a limited region. A schematic diagram in Figure 21 illustrates the idea of partial axial deformation caused by single stiffener within an effective width. Instead of using the total width, the region dominated by stiffeners is effectively causing the bending. In fact, the strain concentration we observed in both surface displacement analysis and finite element analysis also implies the localized in-

plane expansion. We figured that the fitting parameter β should actually be coming from this modifier of effective width. The modified analytical model is written as equation (3).

$$\kappa(\Phi_0) = \frac{1}{\rho} = \frac{\delta \frac{\dot{\alpha}\dot{\alpha}_0}{2E_1} \Phi_0^{\,2}}{\frac{2}{h}\left(E_1 I_1 + E_2 I_2\right)\left(\frac{1}{E_1 a_1 w_1} + \frac{1}{E_2 a_2 w_{eff}}\right) + \frac{h}{2}} \tag{3}$$

In fact, from Figure 19, we observed that each stiffener contributes certain extra region in addition to its own width. In other words, multiple stiffeners are able to contribute more localization and constrain larger region of in plane deformation. This gives us higher value of effective width that actually involves bending and leads to larger actuation curvatures.

To understand the relation between effective region and stiffeners, we utilized the developed finite element framework to perform series of simulations on a 3-cell DEA with single stiffener of different width. The thickness of series of stiffeners are changed according to different width to maintain the same bending stiffness. In Figure 22, width of the single stiffener was changed from 0.75mm to 4mm and we can see the curves of decaying localized strain in all cases are following the same trend. This imply the effective width contains the width of stiffener itself and an additional region surrounding it which is independent to the stiffener's width. That is to say, the effective width can be written as $w_{eff} = w_{stiffener} + w_{sealing\ \ region} + (2n) w_{localiztion}$, where $w_{stiffener}$ is the total width of stiffeners,

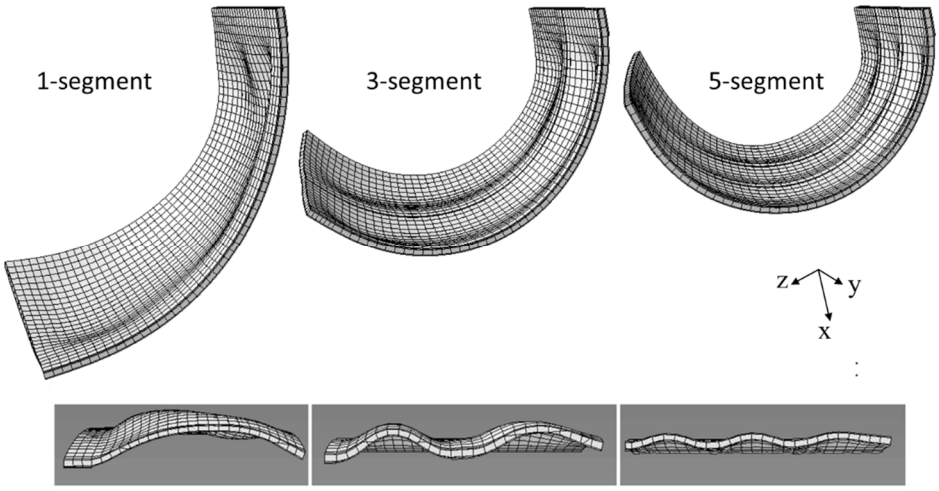

Figure 20. Side view and cross-sectional view of half sample of 3-cell actuator attached with 1, 3, and 5 segments of stiffeners in finite element simulation under applied nominal electric field of 22400 V/mm.

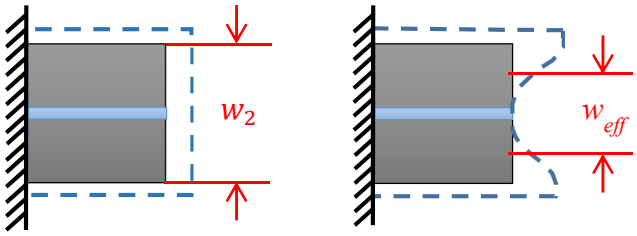

Figure 21. Schematic diagram of narrow strip stiffener constrains only part of the axial expansion of EAP. (a) In ideal case of analytical solution, uniform in-plane expansion of EAP is expected. Total EAP width, w2 are affected by stiffener. (b) In real case, only partially constraint is caused by narrow stiffener reinforcement and weff is required to replace w2.

$w_{sealing\ \ region}$ is the sealing region from the actuator design which is 3mm total, , and $w_{localiztion}$ is the local constraint width caused by each stiffener. For cases with multiple stiffener, n is the number of stiffeners where $(2n)$ describes the surrounding region on both side of the stiffeners. In this case, we found the $w_{localiztion}$ is equal to 2.5mm. Applying this to our analytical model for the splitting stiffener samples, the compared results with experiments are show in Figure 23.

Theoretically, effective width can be increased indefinitely; however, after certain amount of stiffeners, the localization effective region caused by each stiffener may become overlapped. The total effective width is going to be saturated with limited actuation presentation. We simulated the effect of increasing the numbers of split stiffeners from one to five in finite element model as shown in Figure 24. The increases of actuation curvatures become smaller each time we split the stiffener into narrower segments. It saturated at four segments under maximum applied electric field of 22.4 kV/mm.

In addition, total elastic energy was obtained from finite element analysis (Figure 25). The results show that the energy is considered as no change with different numbers of stiffener we use. The energy does not increase with higher actuation curvatures. This indicates that only the efficacy of energy is changing. Actuation strain is more properly used in the bending direction in multiple-stiffener case and leading to higher bending curvatures.

Finally, force-stroke characteristics can also be obtained from finite element simulation. Take applying electric field of 20.8 kV/mm as an example which shown in Figure 26, the increases of stiffener periodicity can be used to adjust different force-stroke characteristics. More stiffeners yield higher blocking force as well as larger deflection of this bending device.

4.4 Conclusion

In this chapter, we studied the role of stiffener in our planar actuator design and provided and promising method to improve actuation performance by tuning stiffener's periodicity. Stiffeners constrained the surface in-plane expansion and induce out-of-plane deformation to planar dielectric elastomer actuators. Each small segment dominated a localized region of in-plane expansion. Experimental and computational results are shown to indicated the strain localization existence and provide evidence of

improving actuation curvatures by tuning the amount of stiffener segments while maintaining the system bending stiffness. A more than 100% of improvement was observed with the proposed optimization with presenting higher device's efficacy. Moreover, force-stroke characteristics can be adjusted by varying stiffener periodicity as well. Modified analytical analysis is also developed to describe and predict the actuator behavior with corresponding actuator geometry and input electric field.

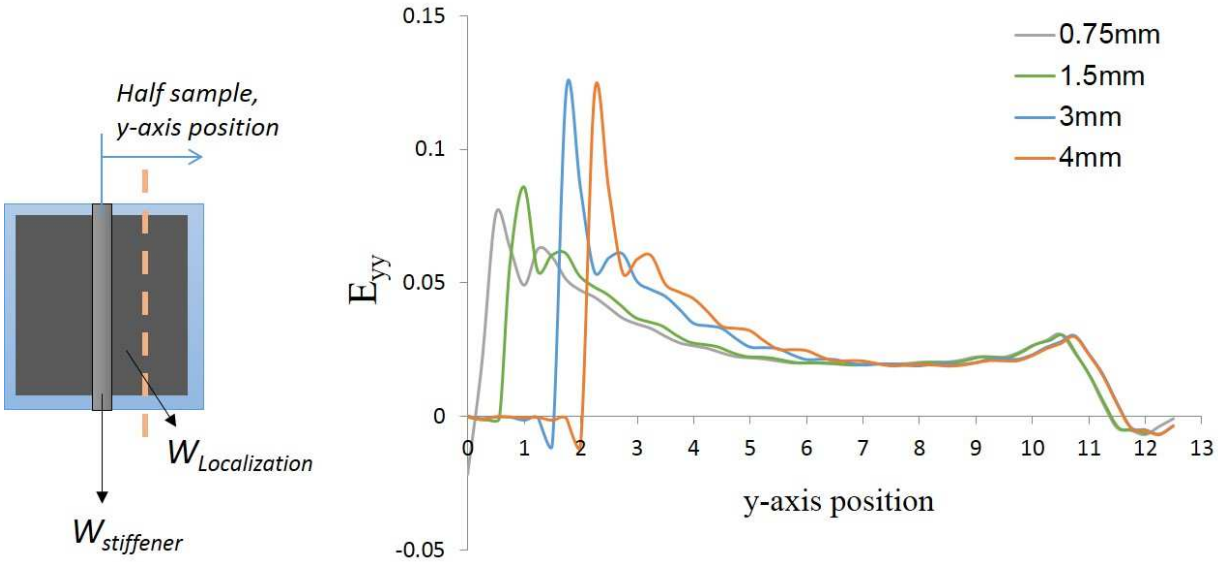

Figure 22. Finite element analysis of strain profiles on lateral direction. Series of modified stiffeners a 3-cell planar dielectric elastomer actuator with width changed from 0.75mm to 4mm while remaining the bending stiffness by changing their thinness accordingly.

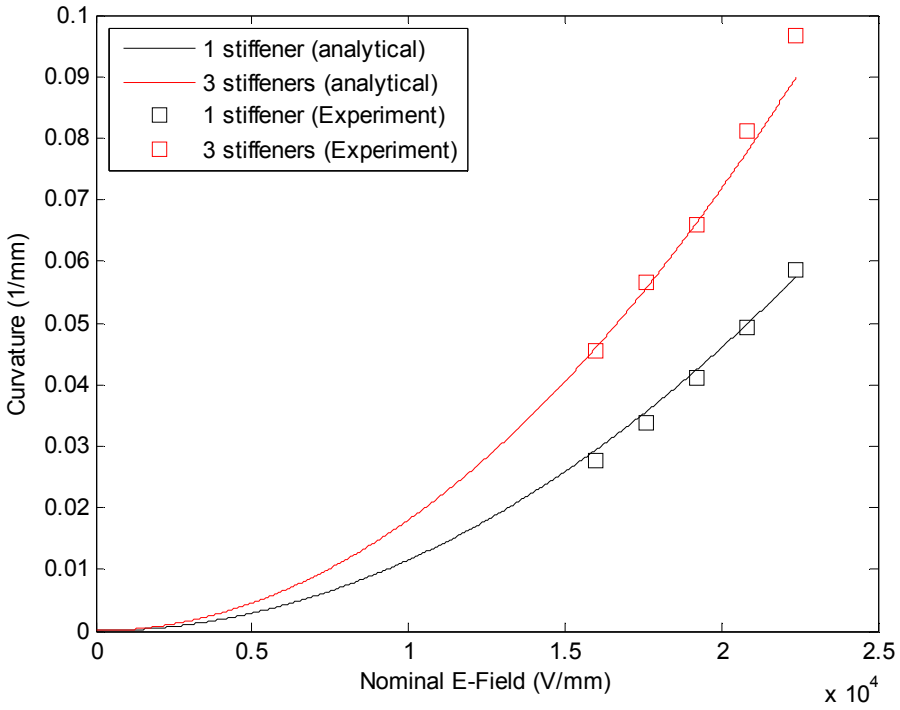

Figure 23. Fitting actuation curvatures from analytical analysis with experimental results. Actuation curvatures shows deformation under applied nominal electric field of 0-22.4kV/mm of 1 (black) and 3 (red) segments of stiffeners. Square marks and solid lines represent experiments and finite element analysis respectively.

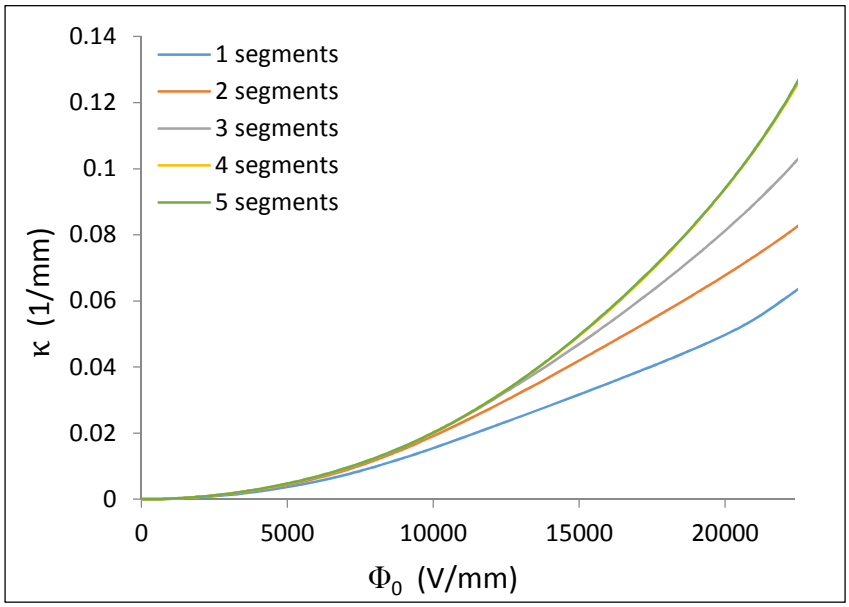

Figure 24. Finite element results of actuation curvature versus applied nominal electric field of 3-cell planar actuator with different numbers of split stiffeners from one to five.

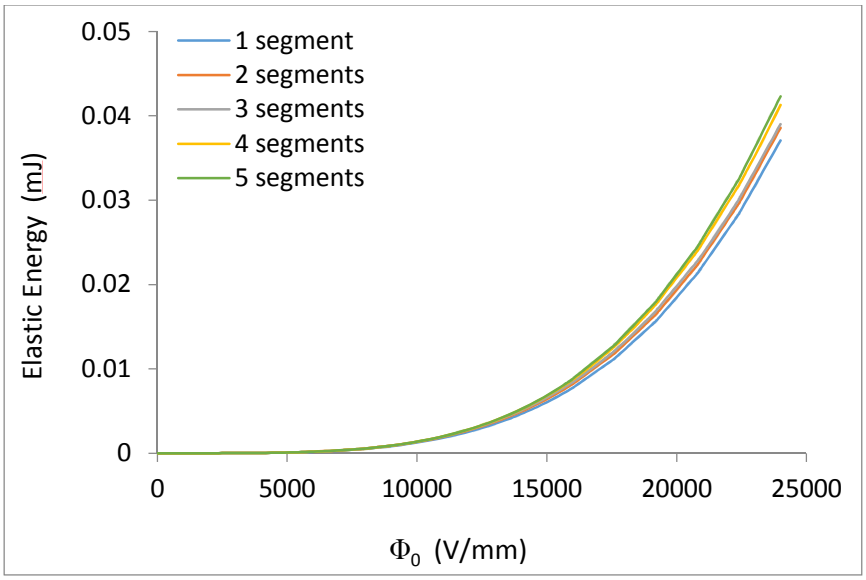

Figure 25. Finite element results of total elastic energy versus applied nominal electric field of 3-cell planar actuator with different numbers of split stiffeners from one to five.

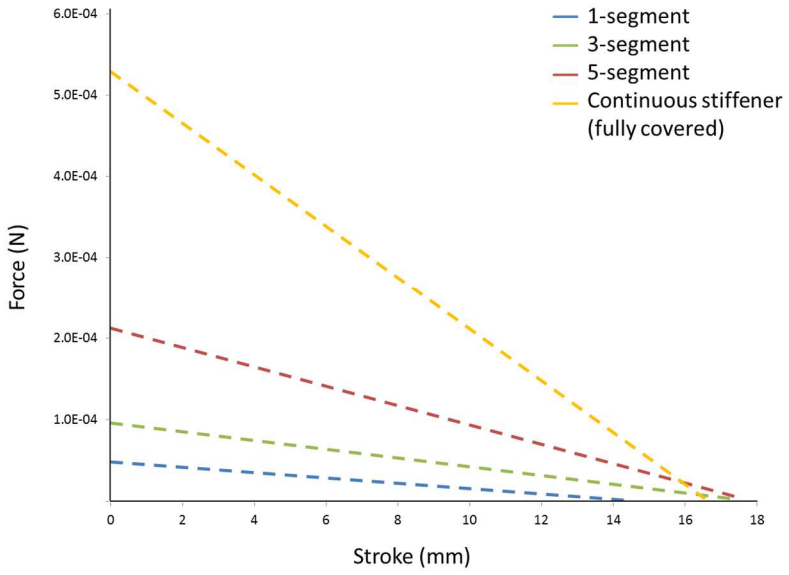

Figure 26. Force-stroke characteristics of 3-cell actuator attached with 1, 3, and 5 segments of stiffeners in Finite element simulation under applied electric field of 20.8 kV/mm comparing with the case of fully covered continuous stiffener.

CHAPTER 5. SURFACE FIBER REINFORCEMENT ON DIELECTRIC ELASTOMER ACTUATORS

5.1 Introduction

In literatures, it shows that birds and bats utilizing flexible wings to replace vertical tails as the flying direction control [31]. This mechanism provides them lighter weight and is able to apply on micro aerial vehicles (MAVs) design for higher energy-to-mass ratio and better efficiency. Bats have especially drown our attention due to their unique wing structure and flying mechanism [43, 86, 87] that benefits the most from aerodynamics. Bat's wing structure is considered as an airfoil [40, 41, 88]. The wing skin is known to be thin and highly deformable to adjust wind flow, yet, stiff enough to carry airflow. In literature [38], the mechanical properties of bat wing membrane was evaluated and shown highly anisotropic [37, 38, 87, 89]. On spanwise direction, the wing membrane is highly compliant with high failure strain, whereas on chordwise direction, some parts of the wing membrane may show a sharp increase at a particular stretch levels and become more than two orders of magnitude higher [41]. From anatomy point of view, the most noticeable feature is their mesh fibrous composite structure which were understood as the combination of collagen and elastic mesh [37, 39, 89]. It is believed that the organic

composite structure provides bat wings the ability of large scale expansion accompanied by a wide range of adjustable stiffness.

In the meantime, dielectric elastomer actuators (DEAs) has been shown their potential in soft robotic device development with their muscle-like features [23, 32, 46, 48, 56]. Since dielectric elastomers are compliant membranes like bat wings and able to demonstrate large deformation with electrical stimulation, we are inspired by bats and interested in applying similar fibrous structure on bat wings to actuator design. In literatures, chemical method induced inter-polymers composites were studied by employing interpenetrating polymer networks [57, 90]. The polymer composite showed high mechanical nonlinearity where the membrane is very compliant at lower stretch level and has a stiffening effect under high stretch. Here, we are seeking of an easier mechanical method to fabricate fibrous elastomer composites. We aim to apply a similar strategy by utilizing additional surface reinforcements with motion flexibility on dielectric elastomers to mechanically stiffen membrane at large stretch, yet, not to sabotage much of current compliancy at lower stretch level for large deformation. This may be an approach to benefit from bat wings behaviors and tune up actuator performance. In this study, mechanical behavior of fibrous elastomer composites with different orientation patterns will be tested. Moreover, we will also be demonstrating the effect of surface fiber reinforcement from the electromechanical coupling aspect to study potential of the design.

5.2 Fiber Electrodes

Replacing electrodes on dielectric elastomer actuators from powder liquid/grease form to fibers, they work not only as conducted layer but also surface reinforcements and constraints. Figure 27 shows the results of preliminary experiments of applying carbon fiber on the surface of prestretched dielectric elastomer membrane. The VHB 4910 tapes were biaxial prestretched with λ=4 and fixed on an outer rigid frame. Electrodes of carbon fibers were distributed on the central of the surface within 1 in x 1 in area and carbon black powders were deposited after to fill up gaps in between fibers and increase conductivity. Sequence of Electric fields were applied through high voltage supply from 0 to 8kV. The results showed that fibers effectively constrained the expansion alone the reinforced direction and allowed deformation on the transverse direction at the same time. The next step is employing different fiber arrangement to study the actuator performance with such surface reinforcements.

5.3 Sample Preparation

To study the effect of surface fiber reinforcement on dielectric elastomer actuators, we fabricated samples embracing a clamp-to-clamp configuration [48, 56]. This configuration fixes the prestretched elastomer membranes laterally on top and bottom

edges with clamps and allows free vertical motion. It is considered as a suitable setup to study unidirectional mechanical and electromechanical behavior of actuators.

Fabrication procedure is illustrated in Figure 28a. 3M VHB 4905 tapes (0.5mm thick) were used as the dielectric elastomer membranes. A piece of VHB tape was stretched 400% on horizontal direction and 300% on vertical direction and fixed on a supporting frame. Four pieces of narrowly-cut unstretched VHB9460 tapes (0.05mm thick) were prepared and attached to both left and right side-edges. The 4 thin side tapes were deigned not to stiffen the actuator compliany, but to prevent possible crack propagation snap through the sample. Clamps from both sides were then used to stack all the components together on top and bottom and left a rectangular gap (152mm x 12.5mm) in the middle region. Carbon grease (MG Chemicals Inc., USA) was brushed on the surface serving as the compliant electrodes. Finally, the finished actuator was detached from the outer supporting frame and left in air for elastomers to relax. In this paper, we presented three different woven fiber patterns for comparison based on their orientation. They were pre-deformed unidirectional on lateral or vertical axis. The samples are illustrated and shown in Figure 28b-1d.

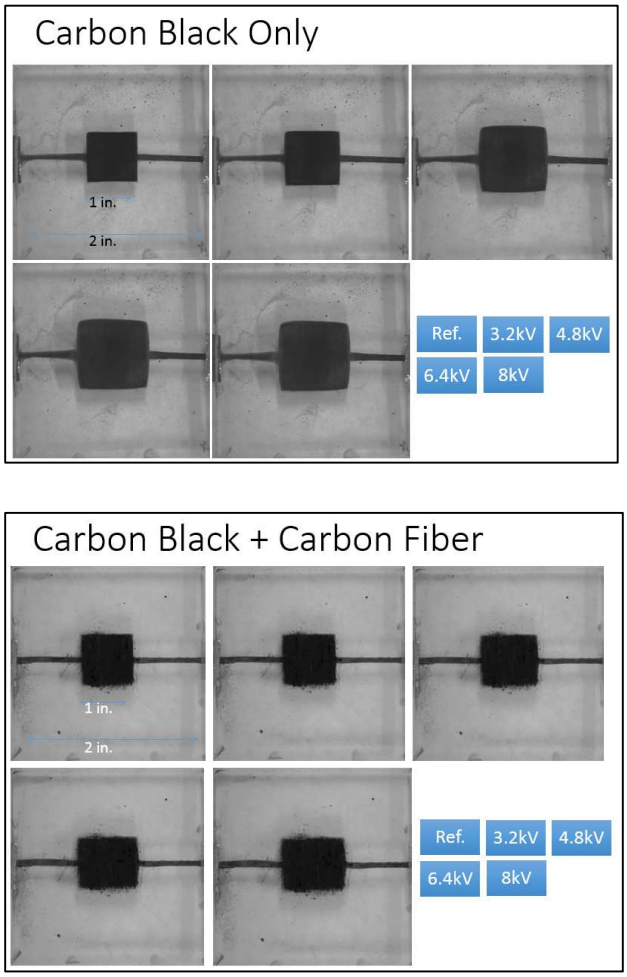

Figure 27. Carbon fiber electrode shows effective constraint of in-plane expansion of dielectric elastomer actuators. Upper sample shows the results of utilizing carbon black powder only, whereas the lower sample shoes the results of utilizing carbon fiber and carbon black.

5.4 Experiment

Mechanical as well as electromechanical tests were both conducted to each sample with different surface reinforcement patterns. Instron testing machine was used to control load and displacement and collect end-point displacement of the samples. To ensure every sample was tested with the same initial stretching condition, the starting stretching state was fixed at stretch of 2 in each attempt. The initial stretches were introduced to each sample by Instron testing stage. Samples were then left under displacement-controlled mode for additional 30 minutes before the major testing for the purpose of eliminating elastomer viscoelasticity via relaxation.

To measure the pure mechanical response, tensile tests were conducted under continuous load with applied loading rate of 0.25N per second. The results of mechanical tests are shown in Figure 29 in a stress-stretch plot. Here, true stress was utilized to represent the respond stress components. They were calculated by using the cross-sectional area at the corresponding deforming instants, the instants thickness was calculated by assuming the material is incompressible and no edge necking effect occurs.

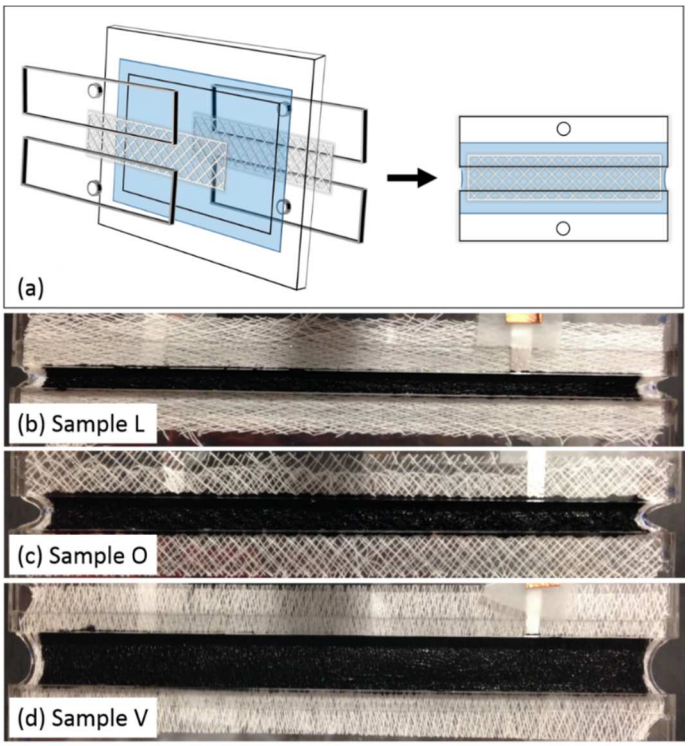

Figure 28. Actuator fabrication procedure (a). Samples of elastomer membrane with different surface fiber reinforcement configurations are shown in (b) (c) and (d). Sample L, O, and V represent different fiber patterns, where L is laterally stretched woven fibers, O is orthogonally arranged woven fibers, and V is vertically stretched woven fibers.

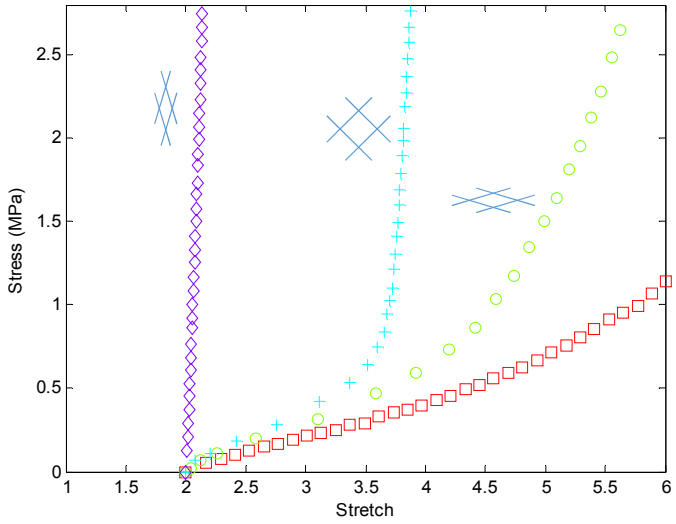

Figure 29. Tensile test results for mechanical property evaluation. Square markers represent the reference sample with no fiber attached. Circle, plus sign, and diamond markers represent different attached fiber patterns, which are respectively (left to right) vertical stretched, orthogonal, and lateral stretched woven fiber sheets.

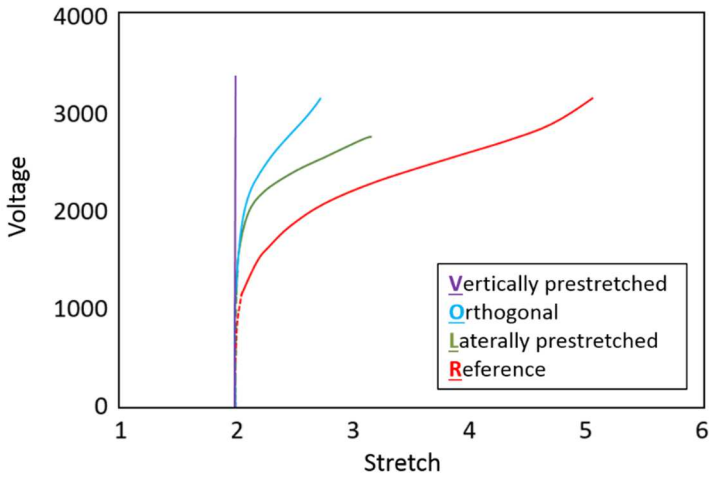

Figure 30. Voltage-stretch plot of electromechanical test results. Overall stiffness changes are observed on the samples with surface fiber reinforcement. The stiffness magnitudes vary with different woven fiber configuration and orientation.

For the electromechanical coupling measurement, the Intron machine was set in load-control mode while the electric field was gradually applied to the testing actuator until failure. The electric field was applied through a slow rate voltage ramp (3.2V per second) devised with a DC-DC converter (Q-80, EMCO Inc.) programed via outlet voltage supply. The test results are shown in Figure 30 in a voltage-stretch plot.

5.5 Discussion

From the experimental results, we observed that fibers in different configurations attributed the level of contribution very differently. Both mechanical and electromechanical characteristics of actuator are highly related to the surface fiber reinforcements. Mechanically, fibrous membranes show noticeable stiffening effect on all three samples with surface reinforcements attached comparing to the reference. Samples with lateral pre-deformed and orthogonal arranged woven fibers are initially in a more compliant state. Fibers were significantly crumbled and provided less contribution at the beginning. With the increases of tensile load, membrane reached the stretch of the fabrication state (stretch of 3) and fibers start to dominantly contribute to the system stiffness. The closer the fiber is orientated to the vertical direction (the loading direction), the larger the stiffness is. This gives us a drastic mechanical property change from the axial modulus aspect before and after the locking point of the fibers. As a matter of fact,

fiber orientation defines the terminal stiffness of the composite membranes. Laminate theory can be employed to predict the equivalent stiffness of fiber reinforced composite in this case. Here in our analysis, the sample structure can be simplified with woven fiber/elastomer/woven fiber sandwich plies stack. Each of the woven fiber plies was considered to be 2 unidirectional fiber plies directly stacked up with fibers pointing to different directions. Fibers are assumed to be aligned one-by-one with only one layer which leads to concentration of $\frac{\pi}{4} \approx 78\%$. For each unidirectional fiber ply, rule of mixture and Halpin-Tsai model [91] were used to calculate equivalent elasticity components on axial fiber direction and transverse direction. More detail of laminate theory model is discussed in appendix D. The fiber orientation here were defined as the angles between fiber and the horizontal axes. By superposing every ply component and assigned fiber angles as listed in Table 1, equivalent modulus of the composite on axial direction were calculated. As a result, the analytical model correspondingly captured the terminal modulus measured from experiments.

Fiber pattern	Fiber angles	Calculated equivalent modulus (GPa)
Lateral stretched	10° and 170°	0.006
orthogonal	45° and 135°	1.2
Vertical stretched	80° and 100°	5

Table 1. Surface fiber orientations and calculated equivalent modulus

On the other hand, electromechanical coupling measurement shows a tradeoff between membrane stiffness and its stretch-ability under actuation. Surface reinforcements introduced higher overall modulus to the system and limited the maximum actuation stretch. Actuation expansion stopped increasing at the designing stretch level which is the prestretch level we applied while attaching fibers on the elastomer during fabrication. Nevertheless, as an exchange of larger deformation, membranes obtained higher stiffness. This may allow reinforced membranes to be applied on wings with the ability to carry larger lifting force comparing to the untreated membranes at the same level of actuation stretch. Comparing to chemical method of synthesizing interpenetrating polymer networks, the mechanical approach is much easier for building a dual stiffness composite membrane. The surface treatment of adding patterned fibers is able to modify membrane's properties and utilized to adjust actuator's performance in different situations and functioning purposes.

5.6 Soft Reinforcement

Noticed from previous section that the fibers applied on actuator surface significantly dominate the system mechanical properties. The property of elastomer membrane can hardly be represented during actuation. Thus, we purpose an idea to lower the modulus of stiffeners in order to present a condition that the properties of both stiffeners and elastomers can be coexisted.

Here, we purpose to utilize the same elastomer material of membrane (3M VHB 4905) as the stiffeners on actuator's surface. Although VHB tapes have much lower modulus compared to the cotton fibers we employed previously, system stiffness will change with the additional thickness by partially adding additional layers on the surface.

To experiment our purposely, we again utilized the clamp-to-clamp configuration for sample fabrication. VHB 4905 tape (0.5mm thick) were used as elastomer membrane. Elastomer membranes were first prestretched 400% on horizontal direction and 300% on vertical direction and fixed on the supporting frames. Two 5mm width VHB 4905 tapes without any pre-deformation were attached on both sides of the edges. Graphite grease was brushed on both surfaces covering up the entire membrane except the stiffener portions. Finally, clamps were assembled to grab the top and bottom edges and support the prestretch of membrane. The finished sample was cut and detached from the supporting frame and let in air for elastomers to relax before testing.

Electromechanical tests were performed to evaluate the coupling effect of soft stiffeners on dielectric elastomer actuators. Intron machine was set in displacement-control mode first to apply initial stretch to the sample for a stretch of 2 and let to relax for additional 30 minutes under displacement-control mode to eliminate elastomer viscoelasticity via relaxation. The loading mode of the testing machine was then changed to load-control while we gradually applied electric field to the actuator until failure. The electric field was applied through a slow rate voltage ramp (3.2V per second) devised with a DC-DC converter (Q-80, EMCO Inc.) programed via outlet voltage supply. The test results are shown in Figure 31 in a voltage-stretch plot.

In the electromechanical test, a very smooth expansion was observed at the beginning of the actuation. The curve trend is corresponding to the result of actuator without any stiffener in our previous work, except slightly shifting upwards. It is expected as the actuator system is slightly stiffened with the additional pieces of VHB elastomers. After the smooth initial expansion via electric field input, a steep stiffening reaction occurred at the level of stretch of 4.6. With increasing the input voltage, actuation response stayed in the stiffened state with limited actuation stretch until reaching the theoretical breakdown point [55, 56] and failed. This shows that by employing softer stiffeners, membrane properties can be retained for a long period until stiffeners start to influence system actuation.

To study how softer stiffeners interact with the actuators, we first attempt to change the stiffeners geometry configuration by doubling the width. The compared results shown in Figure 31 indicates that by increasing the width of stiffeners, a further system stiffening resolved. The actuation curve shifts further upwards and turns into steep region in the earlier stage.

Secondly, we attempt to change the stiffener patterns by splitting them into smaller pieces. We modified two 5mm stiffeners in to five 2mm segments while keeping the same total width. The results of utilizing spreading stiffeners on actuator surface are shown in Figure 32 where a much earlier actuation failure is observed. The actuation performance of both cases follow the identical trend during the smooth expansion region because of the same system stiffness. However, the actuator with spread stiffeners failed at a much earlier stage. This may be due to the giant localized actuation mismatch occurred at the interface of stiffeners and membranes [56, 58, 61]. The localized non-uniform deformation at the junction may lead to instability and cause the failure especially the membrane is under prestretch.

In order to study the possible effect caused by the prestretch on elastomer membrane, we purpose to fabricate actuators at different membrane prestretch level while attaching the stiffeners. Three samples were fabricated under stretch of 2, 3, and 4 for comparison. The samples were left in the air for relaxation after detached from the supporting frame. Before the electromechanically testing, each sample was stretched to

the level of stretch of 2 left on the testing stage under displacement control mode for 30 minutes to eliminate the effect of viscoelasticity. The performance results are shown in Figure 33.

In Figure 33, the first thing we observed is the downward shifting of curves as we introduced higher prestretch to the substrate membrane during fabrication. This indicates a softer system response with the changes which can be explained by using a simple illustration in Figure 34. Because the stiffeners were attached on the substrate membrane while the membrane was under higher stretch comparing to the initial testing stretch, they will be experiencing compression caused by the membrane shrinkage to a lower stretch level. Since the stiffeners need to be straighten or stretched before introducing stiffening effect, during actuation, the system will initially undergo a period of time without the full contribution of stiffeners.

5.7 Conclusion

In summary, this chapter showed how woven fibers affect characteristics of dielectric elastomer actuators both mechanically and electromechanically. Experimentally, actuator stiffness changes were observed for up to four orders of magnitude. The embedded fiber orientation controlled the level and the starting point of stiffness changes. A trade-off between the actuator stiffness and its stroke could be

achieved during the fabrication stage by either the fiber orientation or the prestretch level of the base elastomer membrane. A simplified model using small-strain composite laminate theory was developed and accurately predicted the composite actuator stiffness. Additionally, it was found that a compliant edge stiffeners had a marked effect on the overall actuator electromechanical response.

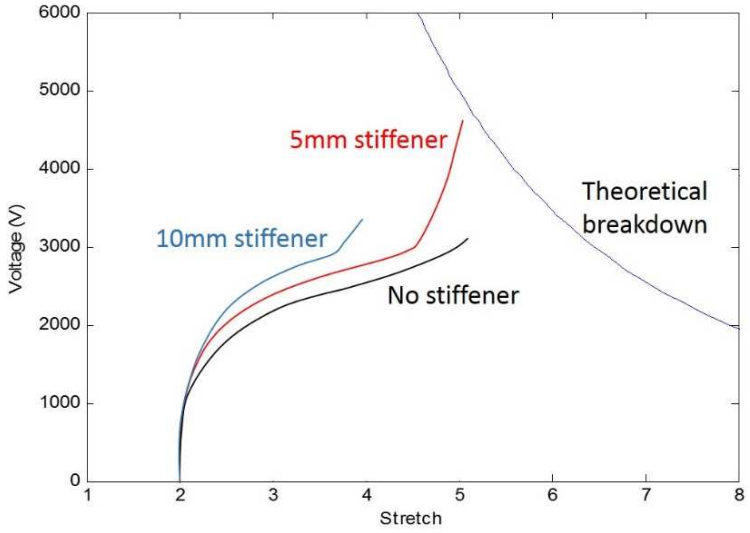

Figure 31. Voltage-stretch plot of electromechanical tests. Three curves (black, red, blue) show the performance of actuators with no stiffener, 5mm stiffeners each sides, and 10mm stiffeners each sides respectfully.

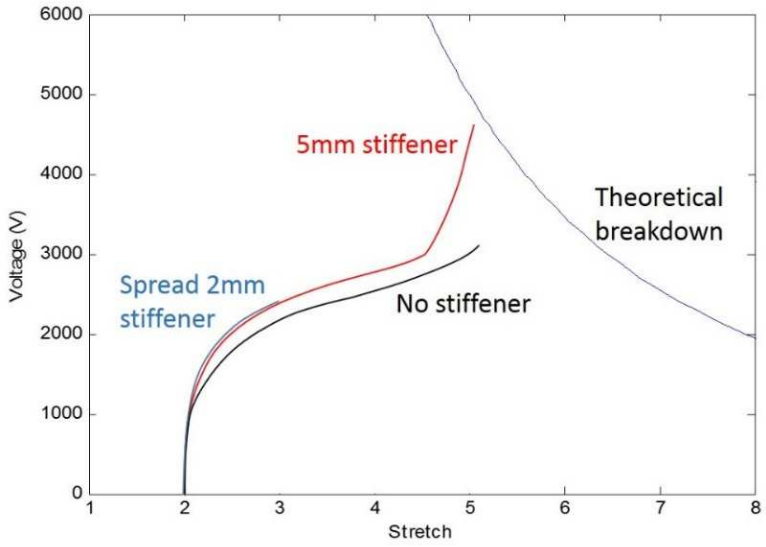

Figure 32. Voltage-stretch plot showing the actuation performance comparison of modified stiffener patterns. The red and blue curves represent the case of 5mm stiffener on both sides and the case of equally spread of five 2mm stiffeners respectfully.

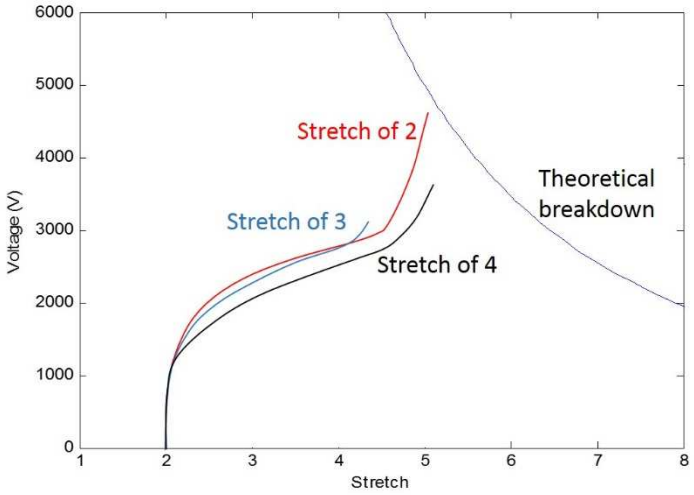

Figure 33. Voltage-stretch plot of actuators with stiffeners attached on membrane substrate under different level of prestretch during fabrication. The red, blue, and black curves represent the prestretch level on membrane of 2, 3, and 4 respectfully.

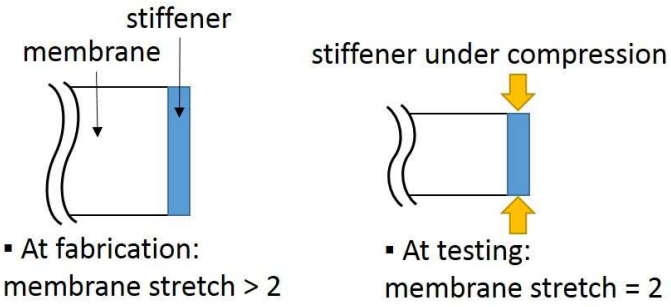

Figure 34. Illustration of interaction between substrate membrane and surface stiffeners under the changes of stretch states.

CHAPTER 6. SUMMARY AND CONCLUSION

In this thesis, the development background of soft actuator was firstly reviewed and the current actuator achievements in literatures were discussed. Different active materials were introduced and electroactive polymers were chosen as the primary materials we employed for actuator development in this work.

To develop soft actuators for MAV applications, we presented a freestanding planar dielectric elastomers actuators design capable of out-of-plane deformation by using patterned surface stiffener reinforcements. This design requires no additional structures to support prestretch that increases the overall flexibility and aims for motion of higher degree of freedom. Experiments were conducted to examine the performance of the actuators. An analytical model was developed according to the experimental results to predict actuation curvatures.

In addition, surface displacement analysis was done by employing digital image correlation technique to understand actuation mechanism and the role of stiffeners. Localized deformation zone was discovered and further investigated through a developed finite element framework with user material subroutine embedded in Abaqus coupling electrical and mechanical responses. As a result, stiffeners are found to be dominating the out-of-plane deformation through localized constrains surrounding each small segment. The characteristics of actuator change with stiffener configuration while

keeping the overall bending stiffness. The efficacy of actuators is greatly improved with the stiffener periodicity and the force-stroke characteristics can be adjusted by varying stiffener configurations as well.

Finally, inspired by the textures on bat wings, a study of utilizing fiber reinforcement on dielectric elastomer actuators were presented showing effected mechanical and electromechanical behaviors. Woven fibers were employed on the surface of actuator membrane with different pre-deformed configurations. Steep stiffness changes were observed in experiments showing the level and the starting stage of stiffness changes are dominated by the applied woven fiber's orientation. The actuator stiffness and its deformability are adjustable with fabrication. The ultimate actuator stiffness of fiber-elastomer composite is predictable accurately by applying a simplified model using small-strain composite laminate theory. Additionally, it was found that a compliant edge stiffeners had a marked effect on the overall actuator electromechanical response. The characteristics of actuator can be modified through stiffener arrangement as well as prestretch level on the elastomer member during fabrication.

REFERENCES

[1] M. L. Levy, A. Nguyen, H. Aryan, R. Jandial, H. S. Meltzer, and M. L. J. Apuzzo, "Robotic virtual endoscopy: Development of a multidirectional rigid endoscope," Neurosurgery, vol. 59, pp. 134-140, Jul 2006.

[2] S. Kim, C. Laschi, and B. Trimmer, "Soft robotics: a bioinspired evolution in robotics," Trends in Biotechnology, vol. 31, pp. 23-30, May 2013.

[3] B. A. Trimmer, H. T. Lin, A. Baryshyan, G. G. Leisk, and D. L. Kaplan, "Towards a biomorphic soft robot: design constraints and solutions," in 4th IEEE RAS and EMBS International Conference on Biomedical Robotics and Biomechatronics (BioRob) / Symposium on Surgical Robotics, Rome, ITALY, 2012, pp. 599-605.

[4] R. Pfeifer, F. Iida, and J. Bongard, "New robotics: Design principles for intelligent systems," Artificial Life, vol. 11, pp. 99-120, Win 2005.

[5] M. Tesch, K. Lipkin, I. Brown, R. Hatton, A. Peck, J. Rembisz, et al., "Parameterized and Scripted Gaits for Modular Snake Robots," Advanced Robotics, vol. 23, pp. 1131-1158, 2009.

[6] W. M. Kier and K. K. Smith, "TONGUES, TENTACLES AND TRUNKS - THE BIOMECHANICS OF MOVEMENT IN MUSCULAR-HYDROSTATS," Zoological Journal of the Linnean Society, vol. 83, pp. 307-324, 1985.

[7] F. Renda, M. Giorelli, M. Calisti, M. Cianchetti, and C. Laschi, "Dynamic Model of a Multibending Soft Robot Arm Driven by Cables," Ieee Transactions on Robotics, vol. 30, pp. 1109-1122, Oct 2014.

[8] H. H. Sun, A. W. Zhao, M. F. Zhang, D. Li, D. P. Wang, L. K. Zhu, et al., "The Analysis model of Torsion Behavior for Octopus-inspired Robotic Arm," in Advances in Bionic Engineering. vol. 461, L. Ren, H. Wang, and Z. Dai, Eds., ed, 2014, pp. 917-923.

[9] B. Mazzolai, L. Margheri, M. Cianchetti, P. Dario, and C. Laschi, "Soft-robotic arm inspired by the octopus: II. From artificial requirements to innovative technological solutions," Bioinspiration & Biomimetics, vol. 7, Jun 2012.

[10] H. T. Lin, G. G. Leisk, and B. Trimmer, "GoQBot: a caterpillar-inspired soft-bodied rolling robot," Bioinspiration & Biomimetics, vol. 6, Jun 2011.

[11] M. A. Simon, W. A. Woods, Y. V. Serebrenik, S. M. Simon, L. I. van Griethuijsen, J. J. Socha, et al., "Visceral-Locomotory Pistoning in Crawling Caterpillars," Current Biology, vol. 20, pp. 1458-1463, Aug 2010.

[12] J. D. W. Madden, N. A. Vandesteeg, P. A. Anquetil, P. G. A. Madden, A. Takshi, R. Z. Pytel, et al., "Artificial muscle technology: Physical principles and naval prospects," Ieee Journal of Oceanic Engineering, vol. 29, pp. 706-728, Jul 2004.

[13] R. F. Shepherd, F. Ilievski, W. Choi, S. A. Morin, A. A. Stokes, A. D. Mazzeo, et al., "Multigait soft robot," Proceedings of the National Academy of Sciences of the United States of America, vol. 108, pp. 20400-20403, Dec 2011.

[14] A. Menciassi, D. Accoto, S. Gorini, and P. Dario, "Development of a biomimetic miniature robotic crawler," Autonomous Robots, vol. 21, pp. 155-163, Sep 2006.

[15] F. Ilievski, A. D. Mazzeo, R. E. Shepherd, X. Chen, and G. M. Whitesides, "Soft Robotics for Chemists," Angewandte Chemie-International Edition, vol. 50, pp. 1890-1895, 2011.

[16] M. Follador, M. Cianchetti, A. Arienti, and C. Laschi, "A general method for the design and fabrication of shape memory alloy active spring actuators," Smart Materials and Structures, vol. 21, Nov 2012.

[17] M. Cianchetti, M. Follador, B. Mazzolai, P. Dario, C. Laschi, and Ieee, "Design and development of a soft robotic octopus arm exploiting embodied intelligence," 2012 Ieee International Conference on Robotics and Automation (Icra), pp. 5271-5276, 2012.

[18] A. Menciassi, S. Gorini, G. Pemorio, P. Dario, and Ieee, "A SMA actuated artificial earthworm," in 2004 Ieee International Conference on Robotics and Automation, Vols 1- 5, Proceedings, ed, 2004, pp. 3282-3287.

[19] H. Yuk, D. Kim, H. Lee, S. Jo, and J. H. Shin, "Shape memory alloy-based small crawling robots inspired by C. elegans," Bioinspiration & Biomimetics, vol. 6, Dec 2011.

[20] A. Antoniou, P. R. Onck, and A. F. Bastawros, "Experimental analysis of compressive notch strengthening in closed-cell aluminum alloy foam," Acta Materialia, vol. 52, pp. 2377-2386, May 3 2004.

[21] W. Tong, "Detection of plastic deformation patterns in a binary aluminum alloy," Experimental Mechanics, vol. 37, pp. 452-459, Dec 1997.

[22] O. A. Araromi, A. T. Conn, C. S. Ling, S. C. Burgess, and R. Vaidyanathan, "A novel fabrication set-up for the flexible production of silicone based EAP "artificial muscle" actuators," Design and Nature V: Comparing Design in Nature with Science and Engineering, vol. 138, pp. 289-300, 2010 2010.

[23] Y. Bar-Cohen, Electroactive Polymer (EAP) Actuators as Artificial Muscles - Reality, Potential and Challenges, 2nd ed. Bellingham, WA: SPIE Press, 2004.

[24] M. Zrinyi, "Intelligent polymer gels controlled by magnetic fields," Colloid and Polymer Science, vol. 278, pp. 98-103, Feb 2000.

[25] H. K. Ju, S. Y. Kim, and Y. M. Lee, "pH/temperature-responsive behaviors of semi-IPN and comb-type graft hydrogels composed of alginate and poly (N-isopropylacrylamide)," Polymer, vol. 42, pp. 6851-6857, Jul 2001.

[26] L. Brannonpeppas and N. A. Peppas, "EQUILIBRIUM SWELLING BEHAVIOR OF PH-SENSITIVE HYDROGELS," Chemical Engineering Science, vol. 46, pp. 715-722, 1991 1991.

[27] B. Kim, K. La Flamme, and N. A. Peppas, "Dynamic swelling Behavior of pH-sensitive anionic hydrogels used for protein delivery," Journal of Applied Polymer Science, vol. 89, pp. 1606-1613, Aug 8 2003.

[28] A. Lendlein and S. Kelch, "Shape-memory polymers," Angewandte Chemie-International Edition, vol. 41, pp. 2034-2057, 2002 2002.

[29] H. Y. Jiang, S. Kelch, and A. Lendlein, "Polymers move in response to light," Advanced Materials, vol. 18, pp. 1471-1475, Jun 6 2006.

[30] A. Lendlein, H. Y. Jiang, O. Junger, and R. Langer, "Light-induced shape-memory polymers," Nature, vol. 434, pp. 879-882, Apr 14 2005.

[31] A. A. Paranjape, S.-J. Chung, and M. S. Selig, "Flight mechanics of a tailless articulated wing aircraft," Bioinspiration & Biomimetics, vol. 6, Jun 2011.

[32] R. Kornbluh, R. Pelrine, and Q. Pei, "Dielectric elastomer produces strain of 380%," in EAP Newsletter vol. 2, ed, 2002, pp. 10-11.

[33] R. Pelrine, R. Kornbluh, Q. B. Pei, and J. Joseph, "High-speed electrically actuated elastomers with strain greater than 100%," Science, vol. 287, pp. 836-839, Feb 4 2000.

[34] X. Zhao and Z. Suo, "Theory of Dielectric Elastomers Capable of Giant Deformation of Actuation," Physical Review Letters, vol. 104, Apr 30 2010.

[35] R. Kornbluh, R. Pelrine, Q. Pei, R. Heydt, S. Stanford, S. Oh, et al., "Electroelastomers: Applications of Dielectric Elastomer Transducers for Actuation, Generation and Smart Structures," in Smart Structures and Materials 2002: Industrial and Commercial Applications of Smart StructuresTechnologies, 2002, pp. 254-270.

[36] M. T. Petralia, R. J. Wood, and Ieee, "Fabrication and analysis of dielectric-elastomer minimum-energy structures for highly-deformable soft robotic systems," in IEEE/RSJ International Conference on Intelligent Robots and Systems, Taipei, TAIWAN, 2010.

[37] K. A. Holbrook and G. F. Odland, "COLLAGEN AND ELASTIC NETWORK IN WING OF BAT," Journal of Anatomy, vol. 126, pp. 21-36, 1978 1978.

[38] S. M. Swartz, M. S. Groves, H. D. Kim, and W. R. Walsh, "Mechanical properties of bat wing membrane skin," American Zoologist, vol. 34, pp. 57A-57A, 1994 1994.

[39] S. Swartz, X. Tian, A. Song, J. Bahlman, and K. Breuer, "Dynamics of bat wing membranes during flight," Bat Research News, vol. 47, p. 151, Win 2006.

[40] A. Hedenstrom, L. C. Johansson, and G. R. Spedding, "Bird or bat: comparing airframe design and flight performance," Bioinspiration & Biomimetics, vol. 4, p. 13, Mar 2009.

[41] S. M. Swartz, J. Iriarte-Díaz, D. K. Riskin, and K. S. Breuer, "A bird? A plane? No, it's a bat: an introduction to the biomechanics of bat flight," in Evolutionary History of BatsFossils, Molecules and Morphology, ed: Cambridge University Press, 2012, pp. 317-352.

[42] K. J. Kim and S. E. Tadokoro, Electroactive Polymers for Robotic Applications, 2007.

[43] J. Colorado, A. Barrientos, C. Rossi, and K. S. Breuer, "Biomechanics of smart wings in a bat robot: morphing wings using SMA actuators," Bioinspiration & Biomimetics, vol. 7, p. 16, Sep 2012.

[44] D. Damjanovic, "Ferroelectric, dielectric and piezoelectric properties of ferroelectric thin films and ceramics," Reports on Progress in Physics, vol. 61, pp. 1267-1324, Sep 1998.

[45] M. H. Lee and H. R. Nicholls, "Tactile sensing for mechatronics - a state of the art survey," Mechatronics, vol. 9, pp. 1-31, Feb 1999.

[46] K. J. Kim and S. Tadokoro, Electroactive Polymers for Robotic Applications: Artificial Muscles and Sensors. London, UK: Springer, 2007.

[47] K. J. Kim and M. Shahinpoor, "Development of three-dimensional polymeric artificial muscles," in Smart Structures and Materials 2001 Conference, Newport Beach, Ca, 2001, pp. 223-232.

[48] M. Shahinpoor, K. J. Kim, and M. Mojarrad, Artificial muscles : applications of advanced polymeric nanocomposites. New York: Taylor & Francis, 2007.

[49] S. Hara, T. Zama, W. Takashima, and K. Kaneto, "Free-standing polypyrrole actuators with response rate of 10.8% s(-1)," Synthetic Metals, vol. 149, pp. 199-201, Mar 31 2005.

[50] T. Mirfakhrai, J. D. W. Madden, and R. H. Baughman, "Polymer artificial muscles," Materials Today, vol. 10, pp. 30-38, Apr 2007.

[51] R. H. Baughman, "Conducting polymer artificial muscles," Synthetic Metals, vol. 78, pp. 339-353, Apr 15 1996.

[52] M. Gerard, A. Chaubey, and B. D. Malhotra, "Application of conducting polymers to biosensors," Biosensors & Bioelectronics, vol. 17, pp. 345-359, May 2002.

[53] K. Oguro, N. Fujiwara, K. Asaka, K. Onishi, and S. Sewa, "Polymer electrolyte actuator with gold electrodes," in Smart Structures and Materials 1999 Conference, Newport Beach, Ca, 1999, pp. 64-71.

[54] S. Liu, R. Montazami, Y. Liu, V. Jain, M. Lin, J. R. Heflin, et al., "Layer-by-layer self-assembled conductor network composites in ionic polymer metal composite actuators with high strain response," Applied Physics Letters, vol. 95, Jul 13 2009.

[55] W. C. Roentgen, "About the Changes in Shape and Volume of Dielectrics Caused by Electricity," Annual Physics and Chemistry Series, vol. 11, 1880.

[56] G. Kofod, R. Kornbluh, R. Pelrine, and P. Sommer-Larsen, "Actuation response of polyacrylate dielectric elastomers," in Smart Structures and Materials 2001 Conference, Newport Beach, Ca, 2001, pp. 141-147.

[57] P. Sommer-Larsen, G. Kofod, M. H. Shridhar, M. Benslimane, and P. Gravesen, "Performance of dielectric elastomer actuators and materials," in Smart Structures and Materials 2002: Electroactive Polymer Actuators and Devices. vol. 4695, Y. BarCohen, Ed., ed, 2002, pp. 158-166.

[58] F. Carpi, P. Chiarelli, A. Mazzoldi, and D. De Rossi, "Electromechanical characterisation of dielectric elastomer planar actuators: comparative evaluation of

different electrode materials and different counterloads," Sensors and Actuators a-Physical, vol. 107, pp. 85-95, Oct 1 2003.

[59] T. Lu, J. Huang, C. Jordi, G. Kovacs, R. Huang, D. R. Clarke, et al., "Dielectric elastomer actuators under equal-biaxial forces, uniaxial forces, and uniaxial constraint of stiff fibers," Soft Matter, vol. 8, pp. 6167-6173, 2012 2012.

[60] J.-S. Plante and S. Dubowsky, "Large-scale failure modes of dielectric elastomer actuators," International Journal of Solids and Structures, vol. 43, pp. 7727-7751, Dec 2006.

[61] W. Lai, "Characteristics of Dielectric Elastomers and Fabrication of Dielectric Elastomer Actuators for Artificial Muscle Applications," MS, Department of Aerospace Engineering, Iowa State University, Ames, IA, USA, 2011.

[62] T. G. McKay, B. M. O'Brien, E. P. Calius, and I. A. Anderson, "Soft generators using dielectric elastomers," Applied Physics Letters, vol. 98, Apr 4 2011.

[63] C. Jean-Mistral, S. Basrour, and J.-J. Chaillout, "Dielectric polymer: scavenging energy from human motion," in Conference on Electroactive Polymer Actuators and Devices (EAPAD 2008), San Diego, CA, 2008.

[64] I. A. Anderson, T. Hale, T. Gisby, T. Inamura, T. McKay, B. O'Brien, et al., "A thin membrane artificial muscle rotary motor," Applied Physics a-Materials Science & Processing, vol. 98, pp. 75-83, Jan 2010.

[65] S. Dastoor, M. Cutkosky, and Ieee, "Design of Dielectric Electroactive Polymers for a Compact and Scalable Variable Stiffness Device," 2012 Ieee International Conference on Robotics and Automation (Icra), pp. 3745-3750, 2012 2012.

[66]

[67] G. Kovacs, L. Duering, S. Michel, and G. Terrasi, "Stacked dielectric elastomer actuator for tensile force transmission," Sensors and Actuators a-Physical, vol. 155, pp. 299-307, Oct 2009.

[68] F. Carpi, C. Salaris, and D. De Rossi, "Folded dielectric elastomer actuators," Smart Materials & Structures, vol. 16, pp. S300-S305, Apr 2007.

[69] A. Wingert, M. D. Lichter, and S. Dubowsky, "On the design of large degree-of-freedom digital mechatronic devices based on bistable dielectric elastomer actuators," Ieee-Asme Transactions on Mechatronics, vol. 11, pp. 448-456, Aug 2006.

[70] P. Lochmatter, G. Kovacs, and P. Ermanni, "Design and characterization of shell-like actuators based on soft dielectric electroactive polymers," Smart Materials & Structures, vol. 16, pp. 1415-1422, Aug 2007.

[71] G. Kofod, M. Paajanen, and S. Bauer, "Self-organized minimum-energy structures for dielectric elastomer actuators," Applied Physics a-Materials Science & Processing, vol. 85, pp. 141-143, Nov 2006.

[72] R. W. Ogden, "LARGE DEFORMATION ISOTROPIC ELASTICITY - CORRELATION OF THEORY AND EXPERIMENT FOR INCOMPRESSIBLE

RUBBERLIKE SOLIDS," Proceedings of the Royal Society of London Series a-Mathematical and Physical Sciences, vol. 326, pp. 565-&, 1972 1972.

[73] G. Kofod, "The static actuation of dielectric elastomer actuators: how does pre-stretch improve actuation?," Journal of Physics D-Applied Physics, vol. 41, p. 11, Nov 2008.

[74] I. Muller and P. Strehlow, "Rubber and Rubber Balloons," ed: Springer, 2004.

[75] A. N. Gent, "A new constitutive relation for rubber," Rubber Chemistry and Technology, vol. 69, pp. 59-61, Mar-Apr 1996.

[76] D. Corbett and M. Warner, "Anisotropic electrostatic actuation," Journal of Physics D-Applied Physics, vol. 42, Jun 7 2009.

[77] L. Tian, L. Tevet-Deree, G. deBotton, and K. Bhattacharya, "Dielectric elastomer composites," Journal of the Mechanics and Physics of Solids, vol. 60, pp. 181-198, Jan 2012.

[78] G. Kovacs, P. Lochmatter, and M. Wissler, "An arm wrestling robot driven by dielectric elastomer actuators," Smart Materials and Structures, vol. 16, pp. S306-S317, 2007.

[79] R. Pelrine, R. Kornbluh, J. Joseph, R. Heydt, Q. B. Pei, and S. Chiba, "High-field deformation of elastomeric dielectrics for actuators," Materials Science & Engineering C-Biomimetic and Supramolecular Systems, vol. 11, pp. 89-100, Nov 2000.

[80] R. Kornbluh, R. Pelrine, Q. Pei, R. Heydt, S. Stanford, S. Oh, et al., "Electroelastomers: Applications of Dielectric Elastomer Transducers for Actuation, Generation and Smart Structures " in Smart Structures and Materials 2002: Industrial and Commercial Applications of Smart StructuresTechnologies, 2002, pp. 254-270.

[81] Q. Pei, M. Rosenthal, S. Stanford, H. Prahlad, and R. Pelrine, "Multiple-degrees-of-freedom electroelastomer roll actuators," Smart Materials & Structures, vol. 13, pp. N86-N92, Oct 2004.

[82] M. Babic, R. Vertechy, G. Berselli, J. Lenarcic, V. P. Castelli, and G. Vassura, "An electronic driver for improving the open and closed loop electro-mechanical response of Dielectric Elastomer actuators," Mechatronics, vol. 20, pp. 201-212, Mar 2010.

[83] S. Timoshenko, "Analysis of bi-metal thermostats," Journal of the Optical Society of America and Review of Scientific Instruments, vol. 11, pp. 233-255, Sep 1925.

[84] W. Lai, A. F. Bastawros, W. Hong, S.-J. Chung, and Ieee, "Fabrication and Analysis of Planar Dielectric Elastomer Actuators Capable of Complex 3-D Deformation," 2012 Ieee International Conference on Robotics and Automation (Icra), pp. 4968-4973, 2012 2012.

[85] M. Aschwanden and A. Stemmer, "Low voltage, highly tunable diffraction grating based on dielectric elastomer actuators - art. no. 65241N," in Conference on

Electroactive Polymer Actuators and Devices (EAPAD) 2007, San Diego, CA, 2007, pp. N5241-N5241.

[86] J. E. Manzo, E. A. Leylek, E. Garcia, and Asme, "DRAWING INSIGHT FROM NATURE: A BAT WING FOR MORPHING AIRCRAFT," Smasis 2008: Proceedings of the Asme Conference on Smart Materials, Adaptive Structures and Intelligent Systems - 2008, Vol 2, pp. 671-678, 2009.

[87] J. W. Bahlman, S. M. Swartz, and K. S. Breuer, "Design and characterization of a multi-articulated robotic bat wing," Bioinspiration & Biomimetics, vol. 8, Mar 2013.

[88] S. M. Swartz, Iriarte-Diaz, J., Riskin, D. K., Song, A., Tian, X., Willis, D., & Breuer, K. S., "Wing structure and the aerodynamic basis of flight in bats," ed: AIAA J, 1, 2007.

[89] I. M. Kovalyova, "The Structure and Functions of the Skin of Bats Flying Membrane (Vespertilionidae, Chiroptera)," Vestnik Zoologii, vol. 42, pp. 525-534, Nov-Dec 2008.

[90] X. Zhao, W. Hong, and Z. Suo, "Electromechanical hysteresis and coexistent states in dielectric elastomers," Physical Review B, vol. 76, Oct 2007.

[91] J. C. HALPIN and J. L. KARDOS, "The Halpin-Tsai Equations: A Review " vol. 16, ed: POLYMER ENGINEERING AND SCIENCE, 1976.

APPENDIX A: FINITE ELEMENT FRAMEWORK

Finite element method is utilized for the computational simulations. User Material subroutine is applied with commercial finite element software ABAQUS. Incompressible Neo-Hookean model is used to represent the elastomer. From literature [90], we know that, elastic energy and electrostatic energy of dielectric elastomer actuator can be written as a function of stretch λ and applied nominal electric field Φ_0 as equation (1) and (2).

$$W_{elastic} = \frac{1}{2}\mu\left(\lambda_1^{\,2} + \lambda_2^{\,2} + \lambda_1^{-2}\lambda_2^{-2} - 3\right) \tag{1}$$

$$W_{\text{electrostatic}} = \frac{1}{2}\dot{o}\dot{o}_0\Phi_0^{\,2}\left(\lambda_1^{-2}\lambda_2^{-2}\right) \tag{2}$$

Therefore, the total free energy can be written in equation (3)

$$W(\lambda_1,\lambda_2,\Phi_0) = \frac{1}{2}\mu\left(\lambda_1^{\,2} + \lambda_2^{\,2} + \lambda_1^{-2}\lambda_2^{-2} - 3\right) + \frac{1}{2}\dot{o}\dot{o}_0\Phi_0^{\,2}\left(\lambda_1^{-2}\lambda_2^{-2}\right) \tag{3}$$

Here, nominal electric field is defined as input voltages used in experiments divided by original thickness between electrode layers of unit cell DEA (0.1mm).

As a result, the two required material properties in our finite element simulation are shear modulus and dielectric constant. Detail of CAD model is discussed in Appendix B.

APPENDIX B: CAD MODEL IN FINITE ELEMENT FRAMEWORK

For the each sample in finite element analysis, we utilized a user material subroutine embedded in Abaqus combined with a constructed CAD model. Each CAD model contains three major parts: (a) active elastomer layer, (b) inactive elastomer layer, and (c) stiffener. Active and inactive elastomer layers are both assigned with dielectric elastomer material properties under user material subroutine with shear modulus of 33kPa (from experimental testing in Chapter 3) and permittivity of $3.21\times8.854\times10^{-12}$ F/m [85]. The thickness of inactive layer is equal to single VHB9460 tape which is 50μm and the thickness of active layer varies with the amount of active cell in each actuator design where each cell is 0.1mm thick. The stiffener part is assigned with isotropic elastic material with Young's modulus of 1.8GPa (from experimental measurement in Chapter 3) and Poisson's ratio of 0.49. The thickness of stiffener layer is 46μm measured from digital deadweight bench gauge. Solid homogeneous section is assigned for all of the parts and an additional field direction (0, 0, 1) is added with user material subroutine to dielectric elastomers. Each layer is linked with surface tie constraints. A Hybrid 20-node quadratic brick element (C3D20H) is employed for each individual layer with nodes seeded 0.5mm apart. In the freestanding-sample simulation, overall structure is based on half model of 3D geometric cantilever laminate by placing roller boundary condition on the symmetric boundary. One edge of the sample is anchored and other edges are left

free-to-move. Curvatures were used to represent actuation motion which is calculated based on the in-plane and out-of-plane displacements of the central point at the end free edge. Nominal electric field is used to assign applied field only on the active region of the active layers. To obtain force-stroke characteristics of actuators, nodes on the far-end edge are tied-up and introduced displacement along the out-of-plane direction together. Each step, electric field and corresponding displacement based on the free-standing tests are applied and the summation of reaction forces of each nodes is calculated to represent the total force output of actuators.

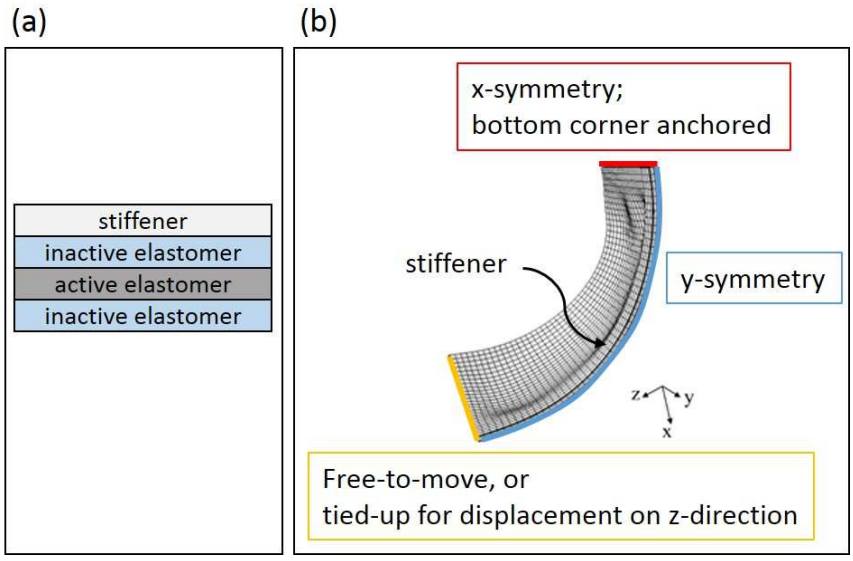

APPENDIX C: HIGH VOLTAGE POWER SUPPLY

High voltage power supply is required to drive a dielectric elastomer actuator. By definition, the Maxwell stress, is proportional to electric field square, which is only related to applied voltage and independent from applied current. In this study, a high voltage amplifier built with a DC-DC converter (Q-80, EMCO Inc.) under minimized current (62.5 μA). It can provide linear amplified output voltages of range of 1.12 - 8kV through 0.7 - 5V input. The corresponding maximum power is low (0.5W) and the overall equipment size is small. The voltage supply circuit is shown as following.

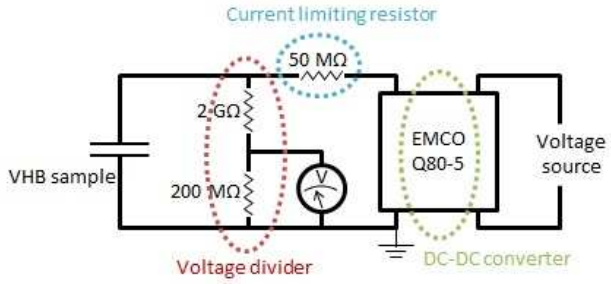

Noted that the threshold voltage for the DC-DC- converter start working is 0.7V; therefore, the output amplified voltage initiates at 1.12kV. Also, the high resisters utilized are for the purpose of dividing high voltage for measurement and protecting system in the event of short circuit. The resisters are, however, too large for commercial multi-meters and results in inaccuracy. In this study, we use an amplifier factor of 1600V provided by the manufactory of the DC-DC converter to convert the amplified applied voltages.

APPENDIX D: LINEAR LAMINATE THEORY FOR FIBER REINFORCED COMPOSITES

Assuming deformation is within elastic region, laminate theory can be employed to predict, design, and analysis the deformation. The hydrothermal expansion can be replaced by corresponding electrical expansion by defining proper coefficients. In chapter 3, the electrical strain written as a function of electric field has been derived in equation 1.

$$\varepsilon_{electrical}(\Phi_0) = \frac{1}{E}\left[\frac{\grave{o}\grave{o}_0}{2}\Phi_0{}^2 - \nu\left(\frac{\grave{o}\grave{o}_0}{2}\Phi_0{}^2 - \frac{\grave{o}\grave{o}_0}{2}\Phi_0{}^2\right)\right] = \frac{\grave{o}\grave{o}_0}{2E}\Phi_0{}^2 \quad (1)$$

By determine electric field square as corresponding temperature change in thermal expansion, the electrical expansion coefficient can be defined. Therefore, for a lamina, k, with its anisotropic mechanical property matrix $[\bar{Q}]$, the stress strain relation can be written in equation 2, where $\{\alpha\}_k$ represents the in-plane electrical expansion coefficient matrix.

$$\{\sigma\}_k = [\bar{Q}]_k(\{\varepsilon\}_k + \{\alpha\}_k \Phi_0{}^2) \quad (2)$$

Combining laminas with elastomers and fibers in various orientations, coupling middle plane stain and curvature, force, and moment can written in equation 3, where the superscripts m and e represent mechanical and electrical terms respectively and $\begin{bmatrix} A & B \\ B & D \end{bmatrix}$ represents coupling matrix calculated from ply modulus matrix.

$$\begin{Bmatrix} N^m \\ M^m \end{Bmatrix} + \begin{Bmatrix} N^e \\ M^e \end{Bmatrix} = \begin{bmatrix} A & B \\ B & D \end{bmatrix} \begin{Bmatrix} \varepsilon_0 \\ \kappa \end{Bmatrix} \quad (3)$$

For a free standing actuator with no external constrain while actuation, the mechanical loads are zero. This makes middle plane stain and curvature of actuator laminate directly calculated from effect carried out from applying electromechanical coupling.

Equilibrium modulus of a fiber-reinforce membrane with woven fibers on the surface is assumed to be stacking multiple layers of unidirectional fiber-reinforce plies with maximum fiber density. Friction and tangling integrations between woven fibers with different orientations are neglected. The result equilibrium modulus is considered as linear superposition of composite layers with applying Hooke's Law.